CHALMERS
UNIVERSITY OF TECHNOLOGY

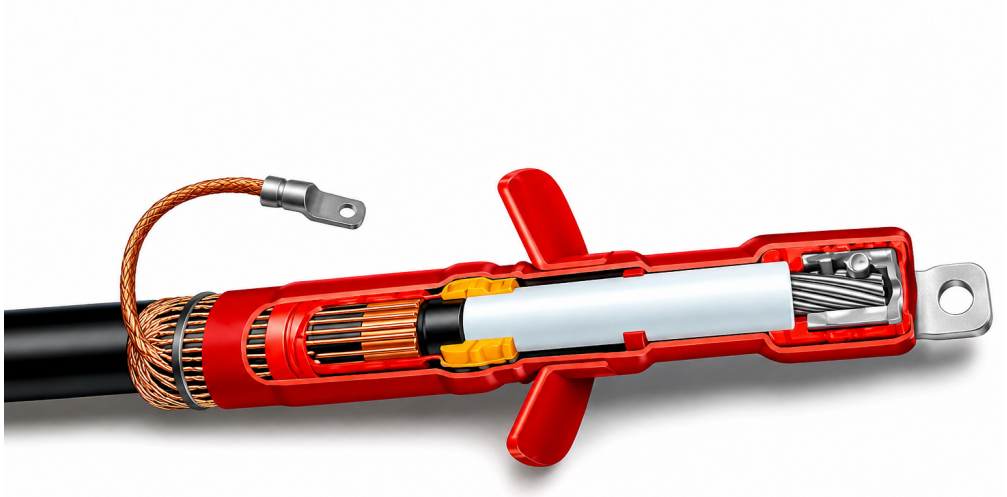

Insulation Assembly Effects on Performance of Medium-Voltage Cable Terminations

Electric Field Analysis

Master's thesis in Sustainable Electric Power Engineering and Electromobility

NAFISEH SAFAEI

DEPARTMENT OF ELECTRICAL ENGINEERING

CHALMERS UNIVERSITY OF TECHNOLOGY
Gothenburg, Sweden 2026
www.chalmers.se

Master's thesis 2026

Insulation Assembly Effects on Performance of Medium-Voltage Cable Terminations

Electric Field Analysis

NAFISEH SAFAEI

CHALMERS
UNIVERSITY OF TECHNOLOGY

Department of Electrical Engineering
Division of Electric Power Engineering
High Voltage Engineering
Chalmers University of Technology
Gothenburg, Sweden 2026

Insulation Assembly Effects on Performance of Medium-Voltage Cable Terminations
Electric Field Analysis
NAFISEH SAFAEI

Supervisor: Mohammad Kharezy, Research institutes of Sweden (RISE)
Examiner: Yuriy Serdyuk, Electrical Engineering

Master's Thesis 2026
Department of Electrical Engineering
Division of Electric Power Engineering
High Voltage Engineering
Chalmers University of Technology
SE-412 96 Gothenburg
Telephone +46 31 772 1000

Cover: Cross-sectional illustration of a medium-voltage cable termination.

Typeset in LaTeX
Gothenburg, Sweden 2026

Insulation Assembly Effects on Performance of Medium-Voltage Cable Terminations
Electric Field Analysis
NAFISEH SAFAEI
Department of Electrical Engineering
Chalmers University of Technology

Abstract

Cable terminations are critical components in medium-voltage (MV) cable systems, where localized electric field enhancement may lead to insulation degradation, partial discharge activity, and premature failure. Sources of the enhanced fields may appear due to improper assembling of the terminations, especially on field conditions. This study investigates electric field distributions in a MV cable termination affected by various types of imperfections using three-dimensional finite element simulations performed in COMSOL Multiphysics. A reference termination model was established to identify critical stress regions and evaluate the influence of termination geometry on the electric field distribution. The effects of semiconductive screen edge geometry, dimensions of stress grading components, air-filled defects, and moisture contamination were systematically investigated. Several defect configurations, including air bubbles, air cushions, and moisture layers at different locations, were analyzed and compared. The results show that the highest electric field concentration occurs near the semiconductive screen cut-back region. A smoother semiconductive screen transition significantly reduced the maximum electric field, whereas moderate reductions in stress grading component length had negligible influence on the field distribution. Among the investigated defects, localized air bubbles and moisture contamination located near the screen cut-back region produced the highest electric field enhancement and therefore the highest risk of electrical overstress and partial discharge initiation. The findings improve the understanding of defect-induced electric field enhancement in cable terminations and provide guidance for improved design, installation, and reliability assessment of medium-voltage cable accessories.

Keywords: medium-voltage cables, cable termination, electric field, COMSOL, partial discharge, insulation defects, stress control.

Acknowledgements

I would like to express my sincere gratitude to my examiner, Professor Yuriy Serdyuk, and my supervisor, Dr. Mohammad Kharezy, for their valuable guidance, insightful discussions, and continuous support throughout this thesis work.
I would also like to express my heartfelt gratitude to my partner. His constant encouragement, motivation, and presence have been a source of strength and inspiration throughout this journey.
Finally, I would like to thank my family for their unconditional love, support, and encouragement throughout my time as a graduate student.

Nafiseh Safaei, Gothenburg, June 2026

List of Acronyms

Below is the list of acronyms that have been used throughout this thesis listed in alphabetical order:

FEA	Finite Element Analysis
FEM	Finite Element Method
MV	Medium Voltage
XLPE	Cross-Linked Polyethelene
EPR	Ethylene Propylene Rubber
PD	Partial Discharge
PDIV	Partial Discharge Inception Voltage
PRPD	Phase-Resolved Partial Discharge
UHF	Ultra-High Frequency

Nomenclature

Below is the nomenclature of indices, sets, parameters, and variables that have been used throughout this thesis.

Parameters

E	Electric field intensity
E_n	Normal component of electric field
E_t	Tangential component of electric field
D	Electric flux density
D_n	Normal component of Electric flux
V	Electric potential
F	Electric force
q	Electric charge
Q_{enc}	Enclosed electric charge
r	Distance between charges
$\hat{r}$	Unit radial vector
ε	Permittivity
ε_0	Vacuum permittivity
ε_r	Relative permittivity
σ	Electrical conductivity
ρ_v	Volume resistivity
U_E	Electric potential energy
L	Semiconductive screen-end transition length

Contents

List of Figures

List of Tables

1
Introduction

1.1 Background

Medium-voltage cable networks constitute a key part of electrical energy distribution systems, operating typically in the voltage range of Um = 1.2 kV to 36 kV. The reliability of these networks depends not only on the cables themselves but also on the performance of cable accessories, particularly terminations and joints. Although medium-voltage cables undergo rigorous factory routine tests, ensuring high theoretical reliability, failures still occur during field operation. A significant proportion of these failures originate from weaknesses introduced during installation. Cable terminations are usually assembled manually under varying field conditions, making workmanship a critical factor. Inadequate installation practices, dimensional deviations, insufficient cleanliness, and improper handling of insulating materials can all lead to dielectric weaknesses. Failure statistics reported in literature consistently demonstrate that termination failures are more frequent than failures in the cable itself. Moreover, environmental conditions such as humidity, contamination, and surface leakage further stress the termination system. Given these factors, cable terminations represent a critical and comparatively weak point in cable systems.

1.1.1 Problem Description and Motivation

Medium-voltage cable systems are widely used in modern electrical power networks due to their high reliability, compact installation, and suitability for urban and industrial applications. Within these systems, cable accessories such as joints and terminations represent some of the most critical components from an insulation reliability perspective. Previous studies have shown that a significant proportion of failures in medium-voltage cable systems originate from cable accessories rather than from the cable insulation itself [1, 2].

Among cable accessories, terminations are particularly sensitive because the original coaxial cable geometry is interrupted at the cable end. In this region, the semiconductive insulation screen is removed and stress grading components are introduced in order to control the electric field distribution. Improper installation, geometrical irregularities, trapped air gaps, contamination, or incorrect positioning of stress grading materials may produce localized electric field enhancement and increase the risk of partial discharge activity and insulation degradation [3, 4, 5].

Since many stages of cable termination assembly are performed manually, the final electrical performance of the termination strongly depends on workmanship quality and adherence to manufacturer installation procedures. Even relatively small defects

introduced during installation may influence the local electric field distribution and create defect-sensitive regions within the insulation system.
Experimental investigation of electric field behaviour inside cable terminations is often difficult due to the complex multilayer geometry and limited accessibility of internal regions. Therefore, numerical simulation methods such as finite element analysis (FEA) provide an effective tool for analysing electric field distribution and evaluating the influence of installation-related defects.
Motivated by these challenges, this thesis investigates the electric field distribution in medium-voltage cable terminations under healthy and defective conditions using COMSOL Multiphysics simulations. Particular focus is given to the semiconductive screen region and stress grading components, where electric field enhancement and defect-related insulation problems are most likely to occur.

1.2 Aim

The aim of this thesis is to investigate the electric field distribution in medium-voltage cable terminations and evaluate the influence of installation-related defects on electric field enhancement and insulation reliability.

1.3 Objectives

The objectives of this thesis are:

- Develop a realistic 3D finite element model of a medium-voltage cable termination.
- Establish a reference electric field distribution for a healthy termination.
- Investigate the effect of assembly-related defects on electric field distribution.
- Identify the most critical defect configurations and locations within the termination structure.
- Assess the influence of defects on electric field enhancement and the associated risk of partial discharge initiation.

1.4 Scope and Limitations

This thesis focuses on medium-voltage cable terminations within the voltage range of 12–36 kV. The investigated geometries and installation configurations are based on selected cable termination sample provided by RISE.
The study primarily investigates the electric field distribution within the termination structure, with particular emphasis on the semiconductive screen cut-back region and surrounding stress grading components. Numerical simulations are performed using COMSOL Multiphysics under frequency-domain conditions.
The investigation is limited to a selected set of assembly-related defects and geometrical variations, including air bubbles, air cushions, moisture-related defects, and variations in stress grading component geometry and semiconductive screen

end. The influence of these defects on electric field enhancement and potential partial discharge risk is evaluated through numerical electric field analysis.

1.5 Methodology

This thesis employs a numerical approach to investigate the electrical behaviour of medium-voltage cable terminations under healthy and defective conditions.
Finite element method (FEM)-based simulations are performed using COMSOL Multiphysics in order to analyse the electric field distribution within the cable termination structure and identify regions of electric field enhancement associated with assembly-related defects. Different defect configurations and geometrical variations are investigated to evaluate their influence on local electric stress distribution.

1.6 Thesis Outline

This thesis is organized into several chapters addressing the theoretical background, numerical modelling, and analysis of medium-voltage cable terminations.
Chapter 1 introduces the background, motivation, objectives, scope, and methodology of the work.
Chapter 2 presents the theoretical background and literature review related to medium-voltage cable systems, cable terminations, electric field theory, stress grading techniques, partial discharge phenomena, and insulation breakdown mechanisms.
Chapter 3 describes the investigated cable termination structure, material properties, numerical modelling approach, boundary conditions, solver configuration, and defect modeling used in the COMSOL simulations.
Chapter 4 presents the corresponding electric field distributions obtained from numerical simulations.
Finally, Chapter 5 summarizes the main conclusions of the thesis and provides recommendations for future work.

2

Theory

2.1 Medium Voltage Cables

Medium-voltage (MV) cables are essential components of modern electrical power systems and are widely used for the transmission and distribution of electrical energy in urban networks, industrial facilities, renewable energy systems, and underground distribution grids. In general, medium-voltage cables operate within the voltage range of approximately 1.2 kV to 36 kV, although the exact classification may vary slightly depending on national and international standards. Their primary function is to transfer electrical power safely and reliably while maintaining sufficient electrical insulation and mechanical integrity under service conditions [6, 7, 8].
Compared with low-voltage cables, MV cables operate under significantly higher electrical stress and therefore require more advanced insulation structures and electric field control methods. The design of MV cable systems must ensure reliable long-term operation under electrical, thermal, mechanical, and environmental stresses [2].
Modern MV cables are generally based on polymeric insulation systems. Earlier cable technologies commonly employed oil-paper insulation, whereas contemporary MV cables mainly use extruded polymeric insulation materials such as cross-linked polyethylene (XLPE) or ethylene propylene rubber (EPR). Among these materials, XLPE has become one of the most widely used insulation materials due to its high dielectric strength, low dielectric losses, favorable thermal performance, and good mechanical properties [8, 9].
A typical MV cable consists of several concentric layers, where each layer performs a specific electrical or mechanical function. Figure 2.1 illustrates the general structure of a medium-voltage cable.

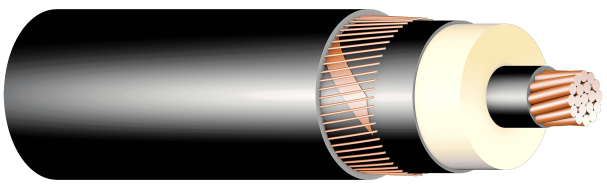

Figure 2.1: Example of medium-voltage cable reproduced from [10].

The conductor, commonly manufactured from copper or aluminium, carries the electrical current. Around the conductor, a semiconductive conductor screen is applied in order to smooth the electric field distribution at the conductor surface and reduce electric field enhancement caused by geometrical irregularities.

The main insulation layer is usually composed of XLPE and provides the primary dielectric insulation between the conductor and the grounded outer layers. Around the insulation, an outer semiconductive insulation screen is installed to maintain a controlled electric field distribution within the cable insulation system.
Outside the insulation screen, a metallic screen or shield is commonly applied using copper wires, copper tapes, or similar conductive materials. This metallic screen is generally connected to ground potential and provides shielding and fault-current return capability. Finally, the cable is protected by an outer sheath that provides resistance against moisture, environmental exposure, and mechanical damage [8, 9].

2.2 Cable Terminations

Cable terminations are critical components of power cable systems and are used to provide the electrical and mechanical transition between insulated power cables and external electrical equipment such as transformers, switchgear, overhead lines, or busbars. The primary purpose of a cable termination is to maintain electrical insulation continuity while ensuring safe electric field distribution at the end of the cable where the insulation system is interrupted [8, 11].
Cable terminations can be classified in different ways depending on their installation environment and insulation technology. Based on the installation location, terminations are generally categorized as indoor or outdoor terminations. Based on the insulation and installation technology, medium-voltage cable terminations may also be classified as heat-shrink, cold-shrink, pre-molded, or tape terminations [11].
Figure 2.2 illustrates the general structure of a heat-shrink medium-voltage cable termination. In addition to stress grading materials, including stress control mastic and atress control tube, cable termination kits commonly include insulating tubes, non-tracking tubes, sealing tapes, breakout boots, and cable lugs [11, 12].

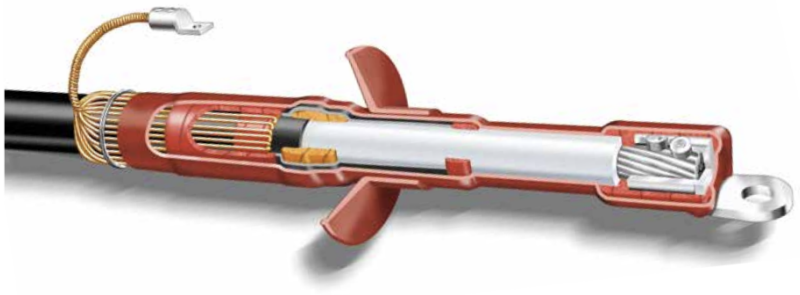

Figure 2.2: Structure of a heat-shrink medium-voltage cable termination [13].

2.2.1 Indoor and Outdoor Terminations

Cable terminations are commonly classified according to their installation environment as indoor or outdoor terminations [8].

Indoor terminations are installed in protected environments such as substations, switchgear rooms, industrial buildings, and indoor electrical installations. Since these installations are relatively protected from direct environmental exposure, indoor terminations are generally more compact and require shorter creepage distances compared with outdoor terminations. In addition, indoor terminations are subjected to lower levels of environmental stress such as rain, ultraviolet radiation, pollution, and surface wetting [8].

Outdoor terminations are designed for exposed operating conditions where the termination may be subjected to rain, humidity, pollution, solar radiation, temperature variations, and other environmental stresses. Therefore, outdoor terminations typically require larger insulation distances and specially designed external sheds in order to increase creepage distance and reduce the risk of surface discharge under contaminated or wet conditions [8].

2.2.2 Heat-Shrink and Cold-Shrink Terminations

Cable terminations may also be classified according to their insulation and installation technology. Among the most commonly used technologies in medium-voltage applications are heat-shrink and cold-shrink terminations [8].
Heat-shrink terminations employ thermally shrinkable polymeric tubes that contract around the cable insulation and termination components when heated by a flame during installation. During the assembly process, heat is applied using a gas torch gun or similar heating device, causing the heat-shrink tubes to recover their original dimensions and tightly conform to the cable structure. Heat-shrink termination systems commonly include stress control tubes, stress grading mastics, insulating tubes, sealing tapes, breakout boots, and outer protective components [8, 12, 14].
One of the major advantages of heat-shrink technology is its flexibility and adaptability to different cable sizes and installation conditions. Heat-shrink terminations are widely used because of their relatively simple installation procedure, good electrical performance, and cost effectiveness [8].

Cold-shrink terminations are based on pre-expanded elastomeric tubes mounted over a removable supporting core. During installation, the supporting core is removed, allowing the elastomeric material to shrink automatically around the cable due to its elastic recovery force. Unlike heat-shrink systems, cold-shrink terminations do not require external heating during installation [8, 14].
Cold-shrink technology generally provides faster installation and reduces the risk of improper heating during assembly. In addition, cold-shrink systems often provide good sealing performance and mechanical flexibility under varying environmental conditions [8].

Besides heat-shrink and cold-shrink technologies, other termination types such as pre-molded and tape terminations are also used in medium-voltage and high-voltage applications. These systems are manufactured with predefined geometries and controlled insulation structures in order to achieve reliable electric field distribution and

mechanical performance [11].

2.3 Electrostatics

Electrostatics is a branch of physics which deals with the phenomena and events of stationary or slow-moving electric charges. In power cable systems operating at industrial frequencies, the electric field behaviour can generally be treated as a quasi-static problem, since electromagnetic wave propagation effects are negligible compared to the geometrical dimensions of the cable system. In electrostatic and quasi-static conditions, the electric field distribution is mainly determined by the applied electric potential, the geometry of the insulation system, and the electrical properties of the surrounding materials, particularly permittivity and conductivity [15, 16].

2.3.1 Electric Field

Electric charges exert forces on one another through the electric field. The interaction between two point charges is described by Coulomb's law, which states that the electric force between two charges is proportional to the product of the charges and inversely proportional to the square of the distance between them,

$$\mathbf{F} = \frac{1}{4\pi\varepsilon}\frac{q_1 q_2}{r^2}\hat{r} \tag{2.1}$$

where $\mathbf{F}$ is the electric force, q_1 and q_2 are electric charges, r is the distance between the charges, $\hat{r}$ is the unit vector defining the direction of the force, and ε is the permittivity of the surrounding medium [15, 17].
The electric field intensity is defined as the electric force acting on a unit positive charge,

$$\mathbf{E} = \frac{\mathbf{F}}{q} \tag{2.2}$$

where $\mathbf{E}$ is the electric field intensity, $\mathbf{F}$ is the electric force, and q is the electric charge. The SI unit of electric field intensity is volt per meter (V/m), which is equivalent to newton per coulomb (N/C) [15].
The electric field is a vector quantity characterized by both magnitude and direction. The direction of the electric field at a given point corresponds to the direction of the force acting on a positive test charge placed at that point. As illustrated in Figure 2.3 electric fields are commonly visualized using electric field lines, which originate from positive charges and terminate on negative charges. The density of these field lines indicates the strength of the electric field. Regions where the field lines are closely spaced correspond to higher electric field intensity. For a continuous charge distribution, the total electric field at a point is obtained by the superposition of the contributions from all individual charges. Therefore, the electric field in practical systems may vary significantly depending on the geometry of the charge distribution and the properties of the surrounding medium.
The electric field distribution is also governed by Gauss's law,

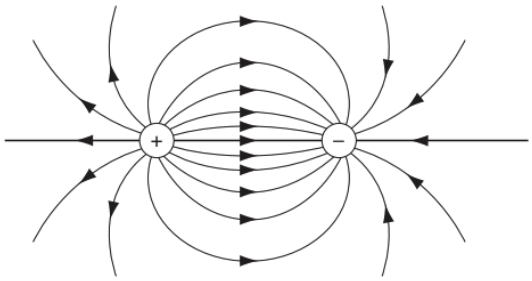

Figure 2.3: Electric field lines between opposite charges [17].

$$\oint_S \mathbf{E} \cdot d\mathbf{A} = \frac{Q_{\text{enc}}}{\varepsilon} \tag{2.3}$$

where Q_{enc} is the total enclosed charge within the closed surface S, ε is the permittivity of the medium, and $d\mathbf{A}$ is the differential surface vector normal to the surface [17]. Gauss's law establishes a direct relationship between electric charge and electric flux, and it forms one of the fundamental equations of electrostatics. In dielectric media, the electric field is influenced by the electrical properties of the material, particularly the permittivity. Different materials respond differently to an applied electric field, leading to variations in field distribution. Consequently, the electric field may become non-uniform in systems containing multiple materials or geometrical discontinuities [16].

2.3.2 Electric potential

Electric potential represents the electric potential energy per unit charge at a given point in space. It is defined as

$$\mathbf{V} = \frac{U_E}{q} \tag{2.4}$$

where $\mathbf{V}$ is the electric potential, U_E is the electric potential energy, and q is the electric charge. The SI unit of electric potential is volt (V) [15].
The electric field is related to the spatial variation of electric potential according to

$$\mathbf{E} = -\nabla V \tag{2.5}$$

where ∇V denotes the potential gradient. The negative sign indicates that the electric field direction points toward decreasing electric potential [17].
This relationship shows that regions with rapid changes in electric potential correspond to regions with high electric field intensity. Consequently, closely spaced equipotential surfaces indicate strong local electric stress [17].

2.4 Electrical Behaviour of Materials

The behaviour of materials under an applied electric field is determined by their electrical properties, primarily conductivity and permittivity. In electrical insulation

systems, different materials respond differently to electric stress depending on the availability of free charge carriers and their ability to become polarized [15, 16].
Based on their electrical conductivity, materials are generally classified into conductors, semiconductors, and dielectrics. Conductive materials allow electric charges to move easily through the material, whereas dielectric materials strongly resist charge transport under normal operating conditions. The interaction between electric fields and material properties plays a fundamental role in determining the electric field distribution within high-voltage insulation systems [17].
In systems containing multiple materials, the electric field distribution becomes dependent not only on geometry and applied voltage, but also on the electrical characteristics of each material. Variations in conductivity and permittivity may produce local electric field enhancement, particularly near interfaces between different materials [16].

2.4.1 Conductive Materials

Conductive materials contain a large number of free charge carriers, typically electrons, which are able to move freely under the influence of an electric field. Due to this high concentration of mobile charges, conductors exhibit high electrical conductivity and allow electric current to flow easily [15, 17].
When an external electric field is applied to a conductor, free charges redistribute rapidly within the material. This redistribution continues until electrostatic equilibrium is reached. Under equilibrium conditions, the internal electric field inside an ideal conductor becomes zero,

$$\mathbf{E} = 0 \tag{2.6}$$

As a consequence, the electric potential throughout the conductor becomes constant, and the conductor behaves as an equipotential body [15].
Since the electric field inside a conductor vanishes at equilibrium, excess electric charges accumulate only on the conductor surface. Furthermore, the electric field at the conductor surface is perpendicular to the surface. Any tangential field component would cause continuous charge motion until equilibrium is restored [17].
The geometry of conductive surfaces strongly influences the surrounding electric field distribution. Sharp edges, corners, and small radii of curvature produce stronger local electric field concentration compared to smooth surfaces [16].

2.4.2 Dielectric Materials

Dielectric materials, also referred to as insulators, contain very few free charge carriers and therefore strongly resist the flow of electric current under normal operating conditions. Unlike conductive materials, electric charges in dielectrics cannot move freely through the material when an external electric field is applied [15].
Although free charge transport is limited, dielectric materials still respond to electric fields through polarization mechanisms. Under the influence of an applied electric field, positive and negative charges within atoms and molecules become slightly displaced relative to each other, producing electric dipoles inside the material [17].

2.4.3 Polarization and Permittivity

When a dielectric material is exposed to an electric field, the internal charge distribution within atoms and molecules becomes distorted. Positive and negative charges are displaced slightly in opposite directions, resulting in the formation of electric dipoles. This phenomenon is known as polarization [15, 17].

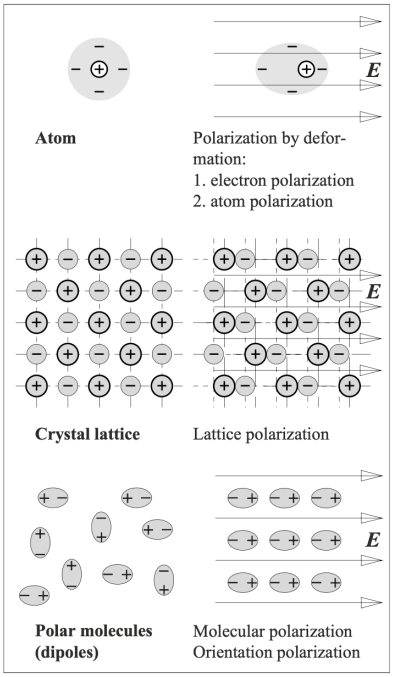

Figure 2.4: Polarization of insulating material under an applied electric field [18].

The collective effect of these dipoles modifies the electric field inside the material. The degree to which a material becomes polarized under an applied electric field is characterized by its permittivity. Materials with higher permittivity can store more electrical energy and generally exhibit stronger polarization effects [15].
The relationship between electric flux density and electric field intensity is expressed as

$$\mathbf{D} = \varepsilon \mathbf{E} \tag{2.7}$$

where $\mathbf{D}$ is the electric flux density, ε is the permittivity of the material, and $\mathbf{E}$ is the electric field intensity.
The permittivity of a material is commonly expressed relative to the permittivity of free space,

$$\varepsilon = \varepsilon_r \varepsilon_0 \tag{2.8}$$

where ε_r is the relative permittivity of the material and ε_0 is the permittivity of vacuum [15].
Polarization mechanisms in dielectric materials may include electronic polarization, ionic polarization, dipolar polarization, and interfacial polarization as illustrated in

Figure 2.4. The dominant mechanism depends on the material structure and the frequency of the applied electric field [18].
Permittivity is one of the most important parameters governing electric field distribution in insulation systems. Variations in permittivity between adjacent materials may produce electric field distortion and localized field enhancement near material interfaces [18].

2.4.4 Electric Field Distribution at Material Interfaces

In practical insulation systems, multiple dielectric materials are often placed together in order to achieve specific electrical and mechanical properties. Since different materials possess different permittivities and conductivities, the electric field distribution within such systems becomes non-uniform [16].
At the interface between two dielectric materials, the electric field distribution is governed by the boundary conditions of electrostatics. For ideal dielectric interfaces without free surface charge, the tangential component of the electric field remains continuous across the interface,

$$E_{t1} = E_{t2} \tag{2.9}$$

while the normal component of the electric flux density also remains continuous,

$$D_{n1} = D_{n2} \tag{2.10}$$

Using the constitutive relation $\mathbf{D} = \varepsilon\mathbf{E}$, the normal electric field components in the two materials are related by

$$\frac{E_{n1}}{E_{n2}} = \frac{\varepsilon_2}{\varepsilon_1} \tag{2.11}$$

This relationship shows that the electric field intensity becomes higher in materials with lower permittivity. Consequently, low-permittivity regions often experience significant electric field enhancement [15, 16].
The electric field distribution in multi-dielectric systems is also influenced by geometry, conductivity, and material interfaces. Sharp geometrical transitions or abrupt changes in material properties may produce localized field concentration. Such field enhancement regions are particularly critical in high-voltage insulation systems because they may initiate partial discharge activity and accelerate insulation degradation [16].

2.5 Partial Discharge

Partial discharge (PD) is a localized electrical discharge that only partially bridges the insulation between conductors and may or may not occur adjacent to a conductor. Partial discharge activity occurs when the local electric field exceeds the dielectric strength of a small region within the insulation system while the overall insulation structure remains electrically intact [16, 18].

In high-voltage insulation systems, partial discharges are generally associated with localized electric field enhancement caused by geometrical discontinuities, insulation defects, material inhomogeneities, or contamination. Repetitive partial discharge activity may progressively degrade the insulation system through chemical, thermal, and mechanical deterioration mechanisms, eventually leading to insulation failure and dielectric breakdown [16].
Partial discharge phenomena are generally classified into corona discharge, internal discharge, and surface discharge according to the discharge location and physical mechanism [16, 18].
Corona discharge occurs in gaseous regions surrounding conductors exposed to highly non-uniform electric fields. Internal partial discharge occurs inside gas-filled cavities, cracks, or defects embedded within solid or liquid insulation materials. Surface partial discharge develops along the surface of insulating materials exposed to air or contaminated environments [18]. Such discharges are particularly dangerous because they are often hidden inside the insulation structure and may progressively degrade the dielectric material over long operating periods [16].

2.6 Stress Grading Techniques

Stress grading is an essential concept in high-voltage insulation systems and is widely used to control electric field distribution in equipment such as power cables, cable accessories, bushings, transformers, and rotating machines [8, 16].
The objective of stress grading is to redistribute the electric field more uniformly and reduce peak electric stress within the insulation system. This is achieved by modifying either the geometry of the insulation structure or the electrical properties of the surrounding materials. Stress grading methods improve insulation reliability by reducing field concentration in critical regions and maintaining a smoother electric potential distribution [8].
Different stress grading techniques are employed depending on the voltage level, insulation configuration, and application requirements. In general, stress grading methods can be classified into capacitive grading, resistive grading, and geometrical stress control techniques such as stress cones. In practical cable accessories, combinations of these methods are often used to achieve effective electric field control and long-term insulation performance [8, 16].

2.7 Breakdown Mechanisms

Electrical breakdown is the failure of an insulating material caused by excessive electric stress, resulting in the formation of a conductive path through the dielectric medium. Breakdown occurs when the electric field exceeds the dielectric strength of the insulation system and the material can no longer maintain its insulating properties [16].
In practical insulation systems, dielectric breakdown is usually preceded by insulation degradation processes such as partial discharge activity, thermal ageing, chemical decomposition, electrical treeing, or surface erosion. Consequently, breakdown

is often considered the final stage of progressive insulation deterioration [18].

2.8 Literature Review

2.8.1 Reliability and Failure Mechanisms of MV Cable Accessories

Medium-voltage (MV) cable accessories, particularly joints and terminations, are widely recognized as the most vulnerable components in underground power cable systems. Several studies have reported that a significant proportion of cable system failures originate from accessories rather than the cable insulation itself [1, 2, 19]. These failures are commonly associated with installation-related defects, thermal stress, moisture ingress, insulation ageing, and electric field enhancement near critical regions such as the semiconductive screen cut-back.

Pompili et al. [1] analysed failure statistics from an Italian distribution network and reported that cable joints account for approximately 57% of failures in MV cable systems. The study further demonstrated that elevated temperature significantly accelerates degradation processes and increases failure rates during summer periods. Similar conclusions were reported by Christou [19], who identified cable accessories as the weakest components in underground networks due to their exposure to combined thermal, electrical, mechanical, and environmental stresses.

Several authors have highlighted that installation quality plays a major role in determining the reliability of cable accessories. Densley [20] explained that defects such as air gaps, contamination, moisture ingress, and interface irregularities may initiate localized electric field enhancement, leading to partial discharge (PD), electrical treeing, and eventual insulation breakdown. Xu [2] further emphasized that approximately 70–80% of failures in MV cable systems occur in accessories such as joints and terminations, primarily due to workmanship-related defects and poor interface conditions.

Experimental investigations have also shown that defects introduced during installation strongly influence insulation degradation. Uydur and Arikan [21] demonstrated that breakdown in aged cable systems frequently occurs within the termination rather than in the cable insulation itself, particularly near stress grading regions. Their results indicated that improper assembly, incomplete semiconductive layer removal, trapped air gaps, and incorrect positioning of stress control materials significantly reduce insulation reliability.

In addition to electrical stress, environmental and operational conditions also contribute to accessory degradation. Pompili et al. [22] showed that increasing temperature reduces the partial discharge inception voltage (PDIV) and increases discharge activity within cable accessories. The study further demonstrated that cavities and interface imperfections create localized high electric field regions that accelerate insulation degradation through PD and electrical treeing mechanisms.

Overall, previous studies consistently demonstrate that cable accessories are critical weak points in MV cable systems, and that installation quality, electric field control, and defect mitigation are essential for improving long-term reliability.

2.8.2 Installation-Related Defects and Workmanship Effects

Several studies have shown that installation-related defects significantly influence the electrical performance of cable accessories and are among the primary causes of premature failure [3, 4, 5, 23]. Since many stages of cable termination assembly are performed manually, the final quality of the installation strongly depends on operator workmanship, surface preparation, and adherence to manufacturer installation procedures.

Tamus et al. [3] investigated repeated failures of a 35 kV cable termination and demonstrated that cavities and interface inhomogeneities created during assembly caused severe local electric field enhancement near the stress control region. X-ray inspection of failed terminations revealed voids and poor adhesion between insulation layers, confirming the critical role of installation quality.

Similarly, Suhaimi and Abd Halim [4] performed post-mortem analysis and finite element simulations of failed cable accessories and identified several common installation defects, including uneven insulation thickness, cuts near the semiconductive screen cut-back region, trapped air gaps, and improper stress control tube positioning. Their results showed that these defects significantly increase local electric field intensity and may initiate partial discharge activity.

Experimental studies further confirm the influence of workmanship on insulation reliability. Suwanasi et al. [23] intentionally introduced different termination defects, including missing stress control components, insulation roughness, improper stress grading positioning, and contamination. The results demonstrated that each defect type produced distinct PD behaviour and significantly reduced the discharge inception voltage compared to properly installed terminations.

Kuusisto [5] investigated installation defects in MV cable joints using both laboratory experiments and COMSOL simulations. The study showed that surface irregularities, air gaps between heat-shrink layers, and incorrect component positioning create localized electric field enhancement that may exceed the dielectric strength of air. Experimental PD measurements confirmed that defective accessories exhibit lower PD inception voltages and higher discharge activity than properly assembled systems.

Recent work by Xin et al. [24] also demonstrated that air gaps formed between cable insulation and stress control tubes represent critical defect locations in cable terminations. Their results showed that interface pressure reduction and defect growth significantly increase electric field intensity and PD activity near the triple junction region.

These studies collectively demonstrate that even relatively small installation-related defects may significantly distort electric field distribution and reduce insulation reliability. Therefore, proper workmanship and accurate installation procedures are essential for reliable operation of MV cable accessories.

2.8.3 Partial Discharge and Diagnostic Techniques

Partial discharge is widely recognized as one of the primary degradation mechanisms in high-voltage insulation systems and is commonly used as an indicator of insulation condition in cable accessories [25]. PD activity typically occurs in regions where

the local electric field exceeds the dielectric strength of the surrounding medium, particularly near voids, interfaces, contamination, or geometrical discontinuities.
Bartnikas [25] provided a comprehensive description of PD mechanisms and explained that discharge behaviour strongly depends on cavity geometry, electric field intensity, space charge accumulation, and material properties. The study also highlighted the importance of phase-resolved PD (PRPD) patterns for identifying different defect types and discharge mechanisms.
Several diagnostic methods have been proposed for detecting PD activity in cable accessories. Chen et al. [26] investigated online PD monitoring using ultra-high frequency (UHF) sensors for MV cable terminations. The results demonstrated that online monitoring can successfully detect PD activity under noisy industrial conditions and identify defects such as residual voids, contamination, and improper stress control installation.
Cselkó et al. [27] compared electrical and acoustic PD measurement techniques for detecting defects in cable terminations. Their results showed that both methods are capable of identifying discharge activity, although electrical measurements provide higher sensitivity while acoustic methods improve discharge localization.
Several studies have also investigated the relationship between PD activity and defect severity. Suwanasi et al. [23] demonstrated that defects such as missing stress control layers and sharp semiconductive protrusions generate significantly higher PD activity than properly installed terminations. Similarly, Uydur and Arikan [21] concluded that PD measurements are more effective than dielectric loss measurements for detecting local termination defects and assessing insulation condition.
Recent studies have further explored advanced PD analysis methods. Xin et al. [24] investigated the evolution of PD behaviour in cable termination air-gap defects and identified several degradation stages based on PRPD characteristics and PD inception/extinction voltages. Uckol et al. [28] proposed a convolutional neural network approach for automatic classification of workmanship defects based on PRPD image analysis.
Overall, previous research confirms that PD activity is closely related to installation-related defects and electric field enhancement in cable accessories. Consequently, PD measurements represent an important diagnostic tool for evaluating insulation condition and detecting early-stage degradation.

2.8.4 Electric Field Simulation and Defect Modelling

Finite element analysis (FEA) and COMSOL Multiphysics simulations are widely used to investigate electric field distribution in cable insulation systems and cable accessories. Numerical modelling provides valuable insight into field enhancement mechanisms, defect sensitivity, and stress distribution in regions that are difficult to evaluate experimentally.
Several studies have demonstrated that insulation defects significantly distort electric field distribution and generate localized stress concentration. Musa et al. [29] investigated the influence of spherical air cavities in XLPE insulation and showed that the electric field inside the cavity becomes substantially higher than in the surrounding insulation due to the large permittivity difference between air and XLPE.

Similarly, Gugulothu et al. [30] analysed the effect of voids, pinholes, and semiconductive irregularities in cable systems using COMSOL simulations. Their results showed that defects located near cable terminations generate strong electric field hotspots that may initiate PD activity and accelerate insulation degradation.
Several investigations have specifically focused on installation-related defects in cable accessories. Suhaimi and Abd Halim [4] demonstrated that air gaps, sharp insulation discontinuities, and improperly positioned stress control materials significantly increase electric field intensity near the semiconductive cut-back region. Similar conclusions were reported by Kuusisto [5], who showed that defects introduced during installation may generate electric field strengths exceeding the dielectric strength of air.
The importance of defect location has also been highlighted in recent studies. Xin et al. [24] demonstrated that air-gap defects near the interface between cable insulation and stress control tubes generate strong electric field enhancement, particularly near triple junction regions. Gugulothu et al. [30] further showed that defect position relative to the conductor and termination structure strongly influences field intensity and insulation degradation.
Despite these advances, many previous studies are based on simplified two-dimensional geometries and assume constant material properties. In addition, interactions between multilayer stress grading materials and realistic three-dimensional defect geometries are often insufficiently investigated. Therefore, further numerical analysis using realistic three-dimensional termination models is required for improved understanding of electric field behaviour in practical cable accessories.

2.8.5 Stress Grading and Electric Field Control

Stress grading is one of the most important techniques used in cable accessories to control electric field distribution and reduce electric stress concentration near the semiconductive screen cut-back region. Without appropriate stress grading, the abrupt termination of the semiconductive layer creates severe electric field enhancement that may initiate partial discharge and insulation failure [31, 32].
Several studies have investigated the influence of stress grading materials on electric field control. Desouky et al. [31] analysed the effect of stress control tube material properties using finite element simulations and demonstrated that high-permittivity materials significantly reduce electric field peaks near the cut-back region. The study further showed that relative permittivity has a stronger influence on field reduction than conductivity.
Batalović et al. [32] also investigated stress control systems using high-permittivity layers and reported that stress grading reduces the electric field from approximately 7 MV/m to 2 MV/m near the dielectric-air interface. Their results confirmed that increasing material permittivity improves electric field uniformity and reduces PD risk.
Väkeväinen [33] investigated the influence of material properties on electric field distribution in cable accessories using COMSOL simulations and experimental validation. The study demonstrated that stress grading materials such as stress control tubes and mastics redistribute equipotential lines and reduce electric field concentra-

tion near geometrical discontinuities. Experimental high-voltage tests further confirmed that properly graded terminations exhibit improved insulation performance and lower PD activity.
In addition to material-based stress grading, geometrical stress control methods such as stress cones have also been investigated. Desouky et al. [31] showed that stress cones redistribute electric field lines and reduce local stress concentration, although these solutions may increase manufacturing complexity and cost.
Overall, previous studies demonstrate that proper stress grading design is essential for controlling electric field distribution and improving insulation reliability in cable accessories. However, many existing studies focus on simplified material systems and do not comprehensively investigate realistic multilayer heat-shrink terminations under installation-related defect conditions.

2.8.6 Research Gap and Motivation

Previous studies have clearly demonstrated that cable accessories such as joints and terminations are among the most failure-prone components in medium-voltage cable systems. assembly-related defects, including air gaps, contamination, improper stress grading, and geometrical irregularities, have been shown to significantly influence electric field distribution and partial discharge activity [3, 4, 5, 24].
In addition, several investigations have demonstrated the importance of stress grading materials and electric field control techniques for improving insulation reliability [31, 32, 33]. Experimental and numerical studies further confirm that localized electric field enhancement near defects may initiate partial discharge activity and accelerate insulation degradation.
However, several limitations remain in the existing literature. Many studies are based on simplified two-dimensional geometries, idealized material properties, or limited defect configurations. Furthermore, realistic heat-shrink termination structures and the interaction between assembly-related defects and multilayer stress grading materials are still insufficiently investigated using three-dimensional numerical modelling.
Therefore, the present thesis focuses on detailed electric field analysis of realistic medium-voltage cable terminations using COMSOL Multiphysics. Particular attention is given to the influence of assembly-related defects and assembly conditions on electric field distribution near the semiconductive screen cut-back region and stress grading components.

3
Method

3.1 Overal Research Methodology

This study uses numerical simulations to investigate the influence of assembly parameters and assembly-related defects on the electric field distribution in medium-voltage cable terminations.
The methodology consists of two main stages:

- Development of a 3D reference model of a medium-voltage cable termination
- Introduction and evaluation of assembly-related defects

3.2 Development of Model in COMSOL

3.2.1 Geometry description

The investigated cable is a three-core medium-voltage power cable, rated for the voltage class 12–17.5 kV. The cable comprises three solid aluminium conductors, each with a nominal cross-sectional area of 150 mm^2. Each conductor is surrounded by an extruded inner semiconductive screen, a layer of XLPE insulation, and an outer semiconductive screen. A concentric copper wire screen with an equivalent cross-sectional area of 25 mm^2 provides the common metallic shielding, and the cable is completed by an outer polymeric sheath for mechanical and environmental protection.

The cable termination investigated in this work is an indoor three-core heat-shrink termination. Based on the cable voltage class and conductor cross-section, the termination designed for three-core medium-voltage cables up to 24 kV. The examined termination is shown in Figure 3.1.
The termination consists of several components, including heat-shrink insulation tubes, outer protective tubes, breakout boots, cable lug, and stress control and sealing materials.
The geometric features of the cable were reconstructed based on direct inspection of the cable cross-section and dimensional measurements obtained from the physical sample. Where applicable, these measurements were verified against the construction principles and dimensional recommendations provided in IEC 60502-2 for medium-voltage cables with extruded insulation [34].

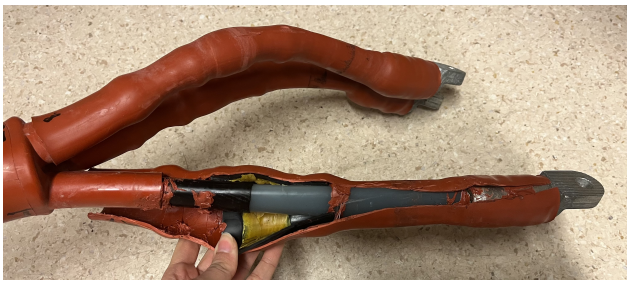

Figure 3.1: Examined termination sample

.

The geometric parameters of the cable and termination used in the model are summarized in Table 3.1.

Table 3.1: Cable and Termination components and dimensional references.

Component	Dimension	Source
Conductor	150 mm^2	Cable marking
Conductor screen	Thickness: 0.5 mm	Measurement
Insulation	Thickness: 4.5 mm	IEC 60502-2
Insulation screen	Thickness: 0.5 mm	Measurement
Metallic screen	25 mm^2 equivalent	Cable marking
Outer sheath of the cable	Outer diameter: 55 mm	Measurement
Outer tube of the termination	Length: 370 mm	Installation instructions
Stress control tube	Length: 90 mm	Installation instructions
Insulating tube	Length: –	–
Breakout boot	Length: 220 mm	measurement
Stress control mastic	Axial length: 30 mm	Installation instructions
Sealing tape	–	Installation instructions
Connector lug	Depth: 60 mm	Installation instructions

The geometric model was developed using a three-dimensional approach based on a combination of direct measurements, manufacturer documentation, and applicable standards. This methodology ensured that the model accurately represents the physical cable and termination configuration and provides a reliable basis for subsequent electric field simulations.

The numerical geometry was developed step by step from the physical cable and termination configuration. First, the cross-section of the cable was examined in order to identify the main cable layers and dimensions. Figures 3.2 and 3.3 illustrate the cross-section of the cable and the external view of the cable, respectively.

The conductor screen, XLPE insulation, and insulation screen were then added as concentric layers around the conductor.

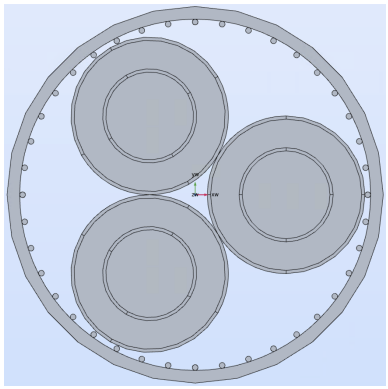

Figure 3.2: Cross-section of the cable

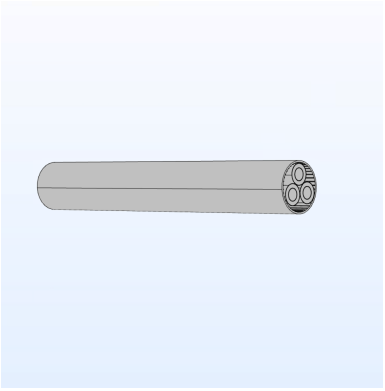

Figure 3.3: Extruded cable

After defining the cable, the termination geometry was added. The first step in the assembly of the cable termination is the removal of the outer sheath of the cable and the separation of the three phases. After this stage, each phase is handled individually and prepared for the installation of the corresponding termination components as Figure 3.4 illustrates.

The modeled termination includes the stress control mastic, stress control tube, outer protective heat-shrink tube, connector lug, and sealing tape. Special attention was given to the semiconductive insulation screen, since this region represents the main geometrical discontinuity in the termination and is expected to experience high electric field concentration. Figure 3.5 presents the complete single-phase termination geometry implemented in COMSOL.

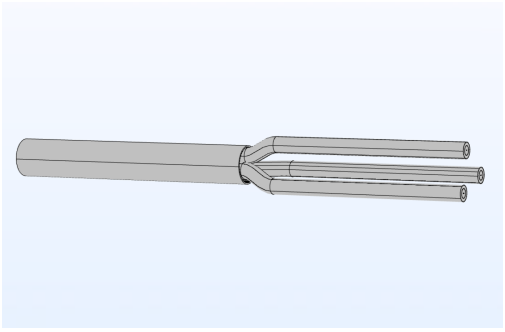

Figure 3.4: Separated phases of the cable

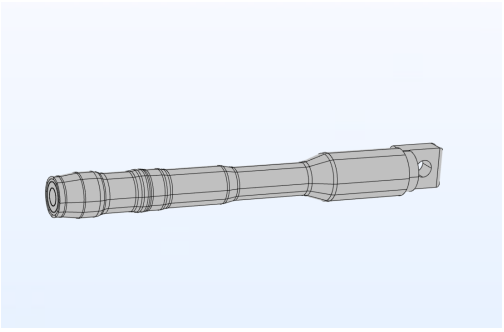

Figure 3.5: Single-phase cable termination

In order to illustrate the internal layer structure of the termination model, a cross-sectional three-dimensional view of the geometry is presented in Figure 3.6. The figure shows the conductor, semiconductive screens, XLPE insulation, stress control mastic, stress control tube, and outer tube included in the simulation model.
A zoomed two-dimensional (2D) view of the critical region in the termination is shown in Figure 3.7.
Particular attention was given to the end of the semiconductive insulation screen, where the original coaxial cable geometry is interrupted. This region,

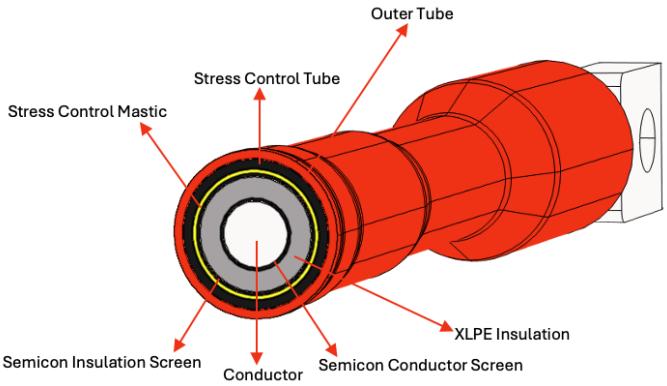

Figure 3.6: Cross-sectional three-dimensional view of the COMSOL model showing the internal components of the investigated cable termination.

commonly referred to in this thesis as the *screen cut-back region*, represents the transition between the grounded semiconductive insulation screen and the surrounding insulation and stress grading materials. Due to the geometrical and material discontinuities present in this region, significant electric field enhancement is expected to occur near the cut-back edge and it was treated as the main region of interest in the simulation.

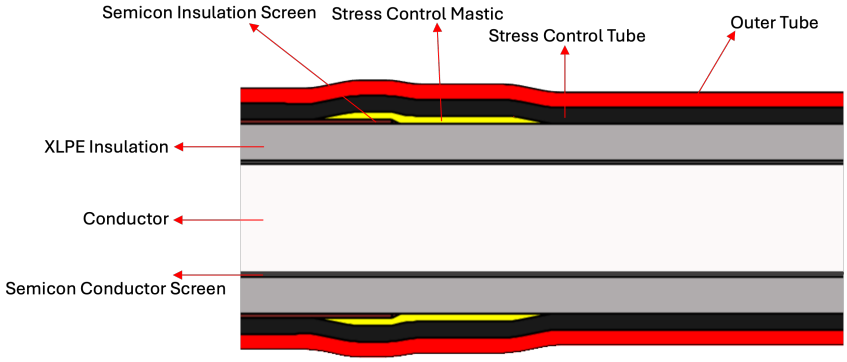

Figure 3.7: Detailed 2D view of the screen end region and stress control components in the COMSOL model.

3.2.2 Material properties

The electrical material properties used in the numerical model were defined based on a combination of manufacturer documentation and values reported in the scientific literature for comparable medium-voltage cable insulation systems and accessories [**?**, 36]. Since the electric field distribution is strongly dependent on the electrical conductivity and permittivity of the materials, particular attention was given to selecting representative values consistent with the actual cable and termination construction.
The electrical conductivity was calculated from the volume resistivity according to

$$\sigma = \frac{1}{\rho_v} \tag{3.1}$$

where σ is the electrical conductivity (S/m) and ρ_v is the volume resistivity (Ω·m).
The cable termination investigated in this work consists of several functional polymeric components. These components are designed to restore the insulation system and control the electric field distribution in the region where the cable semiconductive insulation screen is removed [12].
The manufacturer installation documentation provides detailed mechanical dimensions and installation procedures but does not specify the electrical properties of the polymeric materials. Therefore, representative electrical properties were assigned based on published literature on medium-voltage cable accessories, particularly the work of Väkeväinen [**?**] and experimental measurements reported by Aarnio [36]. These values correspond to typical properties of polymeric insulating, semiconducting, and stress grading materials used in heat-shrink termination systems.
The insulating tubes and outer protective components are composed of polymeric insulating materials characterized by high volume resistivity and low electrical conductivity, ensuring minimal leakage current and maintaining dielectric integrity [**?**]. In contrast, the stress control tube and stress control mastic are formulated as resistive field grading materials with significantly higher conductivity and permittivity than the main insulation. This enables controlled redistribution of the electric field in the screen end region and reduces local electric field enhancement [**?**, 36].
The sealig tape is primarily intended to provide environmental sealing against moisture ingress but also contributes electrically as a weakly conductive insulating material [12].
The electrical properties used in this model are summarized in Table 3.2.
These values provide a realistic representation of the electrical behavior of the termination and allow accurate simulation of electric field distribution, particularly in the stress grading region.

3.2.3 Meshing Strategy

The accuracy of finite element analysis strongly depends on the quality of the computational mesh. In this study, a three-dimensional mesh was generated in COMSOL Multiphysics in order to accurately capture the electric field distribution within the cable termination.
Due to the geometric complexity of the model, including curved geometries, multilayer structures, and thin material regions, a fully physics-controlled mesh could not be applied effectively. Therefore, a user-controlled meshing strategy was adopted, where different mesh types were assigned to different parts of the model depending on their geometrical characteristics. Swept meshes were applied in regions with extruded geometries, while mapped meshes were used on regular surfaces where applicable. In geometrically complex re-

Table 3.2: Electrical properties of materials used in the termination model

Material	ε_r	ρ_v	σ
Aluminium (conductor)	1.0	–	3.774×10^7
XLPE (insulation)	2.3	1.0×10^{14}	1.0×10^{-14}
Semiconductive PEX (screens)	10	1.0	1.0
PE (Outer sheath of the cable)	2.3	1.0×10^{14}	1.0×10^{-14}
Stress control tube	35	1×10^7	1×10^{-7}
Stress control mastic	15	1×10^8	1×10^{-8}
Insulating tube	3.4	1×10^{11}	1×10^{-11}
Sealing tape	3.3	1×10^{10}	1×10^{-10}
Outer tube of the termination	2.5	1×10^{14}	1×10^{-14}
Air (Defect)	1	1×10^{12}	1×10^{-12}
Moisture (Defect)	80	1×10^2	1×10^{-2}

gions, free tetrahedral elements were employed to ensure proper discretization of the model.
Since strong electric field gradients are expected near the semiconductive screen cut-back region and surrounding stress grading components, local mesh refinement was applied in these critical areas. Particular attention was given to the termination of the semiconductive insulation screen, the interface between the XLPE insulation and the stress control materials, and nearby geometrical transitions. A locally refined mesh was therefore implemented in these regions, as shown in Figure 3.8, while a coarser mesh was maintained in less critical regions in order to reduce computational cost.

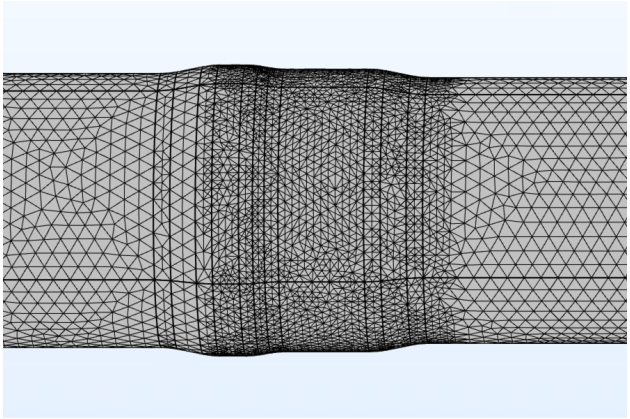

Figure 3.8: Locally refined mesh applied near the semiconductive screen cut-back region and stress grading components.

This meshing strategy allowed the model to capture the key physical phenomena associated with electric field concentration while maintaining a computationally manageable number of elements. The adopted mesh therefore

represents a compromise between numerical accuracy and computational feasibility.

3.2.4 Boundary Conditions

The investigated cable sample belongs to the 12/17.5 kV voltage class. Therefore, an electric potential of 12 kV was applied to the conductor in the model, representing the phase-to-ground operating voltage of the cable system.
Ground potential was assigned to the metallic copper wire screen surrounding the cable insulation. In practical medium-voltage cable systems, the copper wire screen is electrically grounded during operation. Since the outer semiconductive insulation screen is electrically connected to the grounded copper screen, the insulation screen is consequently maintained at ground potential.
The surrounding air region was represented using a computational air domain. The external boundaries of the surrounding air box were assigned ground potential in order to define the reference potential of the model and limit the computational domain.

3.2.5 Solver Configuration

The electric field simulations were performed using the *Electric Currents* interface in COMSOL Multiphysics. A frequency-domain study was employed in order to represent the steady-state AC operating conditions of the cable system at 50 Hz.
The governing equations were solved using a direct linear solver to improve numerical stability and convergence for the multilayer cable termination geometry containing materials with significantly different electrical conductivities and permittivities.

3.3 Defect Modelling

3.3.1 Geometrical Variations

Geometrical variations associated with the termination assembly process were investigated in order to evaluate how dimensional and geometrical changes influence the electric field distribution near the critical stress grading region.

3.3.1.1 Variation in Semiconductive Screen End Geometry

In practical cable termination installation, the geometry of the semiconductive screen end may vary depending on cutting precision, workmanship, and preparation techniques. Variations in the transition geometry at the semiconductive screen end may influence the electric field distribution by modifying the local field grading conditions near the critical stress control region.
In this study, the influence of the semiconductive screen end geometry was investigated by varying the slope transition length, denoted by L, at the screen

cut-back region. The parameter L represents the horizontal transition length between the semiconductive screen edge and the XLPE insulation surface, as illustrated in Figure 3.9.

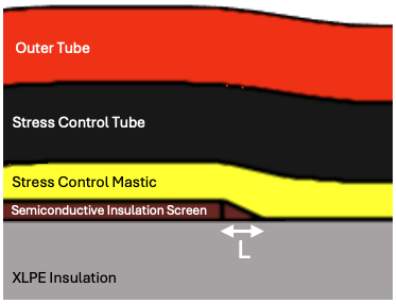

Figure 3.9: Definition of the investigated slope transition length L at the semiconductive screen end.

Several geometrical configurations with different slope transition lengths were introduced in the model in order to evaluate the influence of the semiconductive screen end geometry on the electric field distribution. The investigated values of the slope transition length L are summarized in Table 3.3.

Table 3.3: Investigated slope transition lengths at the semiconductive screen end.

Case	L (mm)
Case S1	0
Case S2	0.5
Case S3 (Reference)	1
Case S4	1.5
Case S5	2

The investigated geometrical variations were selected to represent possible differences in cable preparation and semiconductive screen cutting during termination assembly.

3.3.1.2 Variation in Stress Control Component Length

In addition to interface-related defects, geometrical variations associated with the dimensions of the stress control components were also investigated. In practical cable termination assembly, the lengths and positioning of the stress control mastic and stress control tube may vary depending on assembly precision, shrinkage behaviour, and assembly tolerances. Such variations may influence the electric field distribution by modifying the extent of the stress grading region surrounding the semiconductive screen cut-back area.
In this study, the influence of reduced stress control component length was investigated by modifying the axial lengths of both the stress control tube and the stress control mastic while maintaining the remaining termination geometry unchanged.

The reference stress control tube length was 90 mm, while a reduced configuration of 45 mm was also investigated. Similarly, the reference stress control mastic length was 30 mm, and an additional reduced configuration of 10 mm was analysed.
Figure 3.10 illustrates the investigated geometrical variations of the stress control tube and stress control mastic.

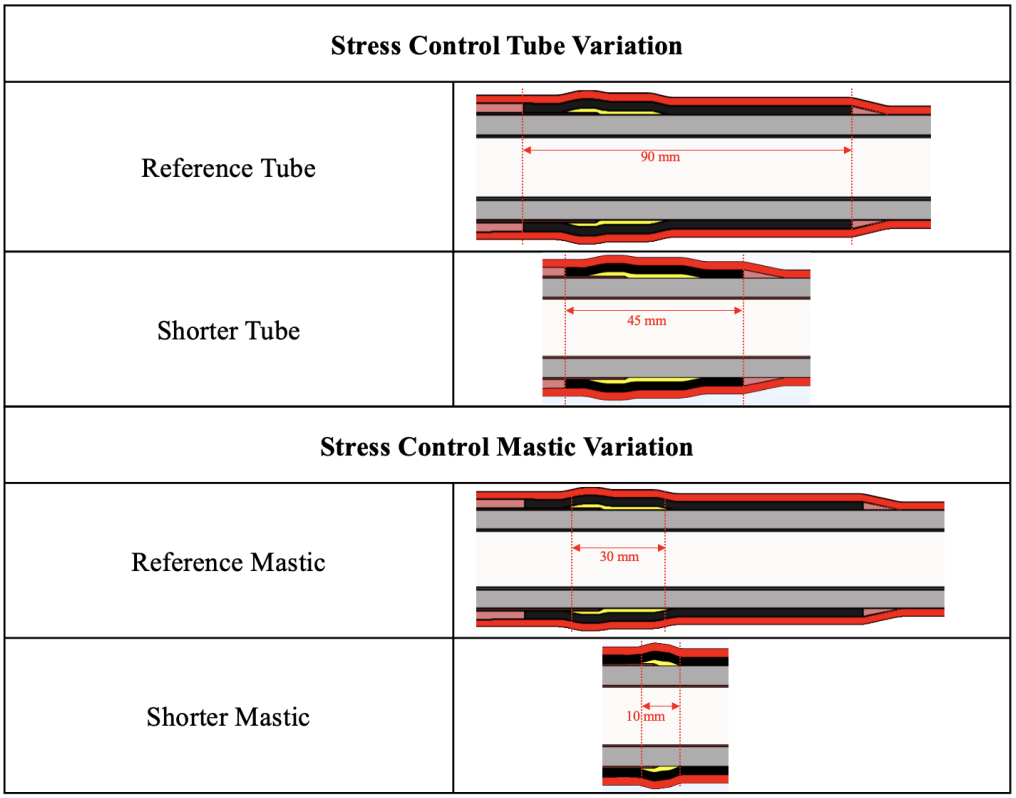

Figure 3.10: Investigated geometrical variations of the stress control tube and stress control mastic lengths.

The investigated configurations were selected in order to represent possible assembly-related dimensional variations caused by insufficient length of stress control materils during termination assembly.

3.3.2 Air Defects

Air defects were introduced into the numerical model in order to investigate the influence of trapped air on the electric field distribution in the cable termination. These defects represent possible assembly-related imperfections that may occur if the heat-shrink stress control materials do not fully conform to the cable surface during assembly. In practice, insufficient shrinkage, uneven heating, surface irregularities, or incomplete contact between layers may leave small air-filled regions at material interfaces or inside stress control components.

Figure 3.11 shows the air defect configurations introduced in the COMSOL model.

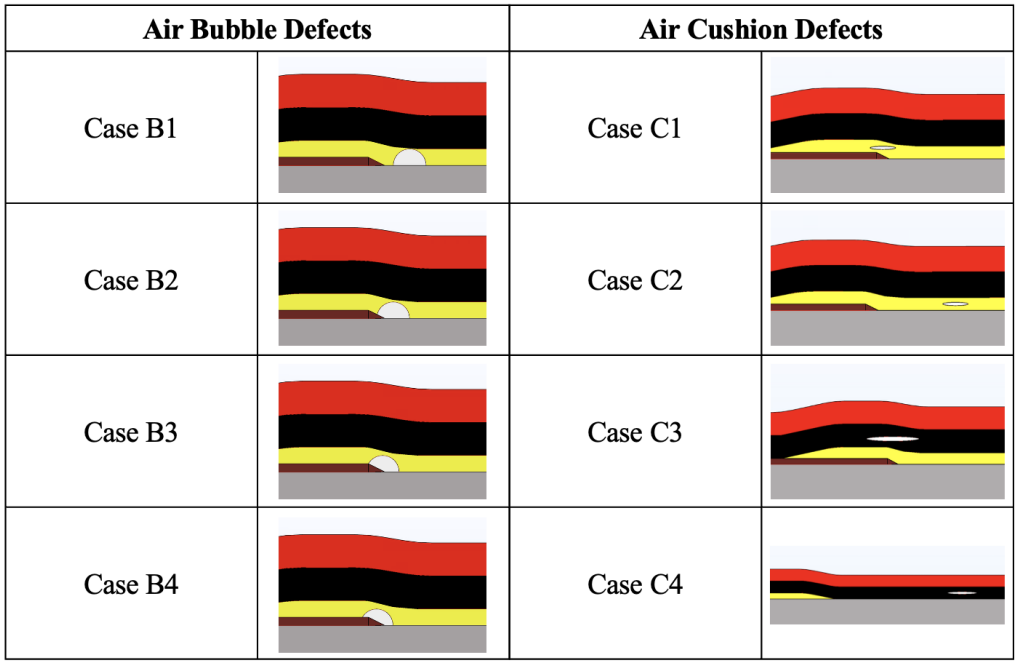

Figure 3.11: Schematic illustration of the investigated air defect configurations introduced in the cable termination model.

Two main types of air defects were considered in this study: air bubbles and air cushions.
The air bubble represents a localized rounded air void located under the stress control mastic, close to the semiconductive screen cut-back region.
The air cushion represents a thin elongated air region formed within the stress control materials, either inside the stress control mastic or inside the stress control tube.
These two defect types were selected because they represent different possible geometrical forms of trapped air caused by imperfect shrinkage or incomplete contact during termination assembly.
The dimensions and locations of the investigated air defects are summarized in Table 3.4. The electrical properties of the air regions were assigned according to Table 3.2.

3.3.2.1 Air Bubble Defects

Air bubble defects were modelled as localized rounded air regions positioned under the stress control mastic near the semiconductive screen cut-back region, as illustrated in Figure 3.11.
The purpose of these cases was to evaluate how trapped air located at critical material interfaces affects the local electric field distribution.
In all air bubble cases, the bubble radius was kept constant at $R = 1$ mm. Different bubble positions were investigated near the semiconductive screen

Table 3.4: Investigated air defect configurations introduced in the COMSOL model.

Defect type	Location	Geometry	Dimension (mm)
Air bubble	Under stress control mastic	Spherical	Radius = 1
Air cushion	Inside stress control mastic	Flattened elliptical	Thickness = 0.25 Length = 2 Width = 1
Air cushion	Inside stress control tube	Flattened elliptical	Thickness = 0.25 Length = 5 Width = 2

cut-back region in order to evaluate the influence of trapped air at critical material interfaces and around the semiconductive screen end.
In Case B1, the air bubble was positioned directly on the XLPE insulation surface at a distance of approximately 1 mm from the semiconductive screen end. In Case B2, the bubble was shifted toward the semiconductive screen cut-back region so that part of the bubble was located above the inclined transition region of the semiconductive screen. In Case B3, the bubble was moved further toward the cut-back region until it was positioned mainly above the inclined semiconductive screen edge. In Case B4, the bubble was shifted even further toward the semiconductive screen so that part of the bubble extended onto the semiconductive screen surface itself.
These configurations were introduced in order to investigate the sensitivity of the electric field distribution to trapped air defects located at different positions around the semiconductive screen cut-back region.

3.3.2.2 Air Cushion Defects

Air cushion defects were modelled as thin oval-shaped air-filled regions inside the stress control materials, as illustrated in Figure 3.11.
Unlike the rounded air bubble defects, air cushions represent flattened air gaps that may develop due to incomplete shrinking of the heat-shrink material during installation..
Different air cushion dimensions were considered for the stress control mastic and stress control tube regions in order to represent more realistic assembly-related trapped air configurations. The air cushions introduced inside the stress control tube were modelled with larger and wider geometries compared with those inside the stress control mastic due to the larger physical dimensions and different shrinkage behaviour of the tube material.
Two locations were considered for the air cushion defects.
In Cases C1 and C2, the air cushions were positioned inside the stress control mastic. In Case C1, the defect was located directly above the semiconductive

screen cut-back edge, corresponding to the region where the insulation screen terminates. In Case C2, the defect was positioned approximately 5 mm away from the semiconductive screen end along the cable axis.
In Cases C3 and C4, the air cushions were introduced inside the stress control tube. In Case C3, the defect was located directly above the semiconductive screen cut-back region, while in Case C4 the defect was positioned approximately 40 mm away from the semiconductive screen end.
These configurations were selected in order to compare the sensitivity of different stress control regions to trapped air defects caused by imperfect shrinkage or insufficient material contact.

3.3.3 Effect of Missing Stress Control Mastic

The stress control mastic plays an important role in cable termination systems by filling geometrical irregularities, eliminating trapped air gaps, and providing a smooth transition between adjacent insulation layers. The screen cut-back region contains geometrical discontinuities that make complete contact between adjacent stress grading components difficult to achieve. If the stress control mastic is omitted during termination assembly, the stress control tube may not fully conform to the underlying geometry, allowing air-filled voids to remain trapped within the termination structure.
Improper installation or accidental omission of the stress control mastic may therefore lead to the formation of air-filled voids underneath the stress control tube.
To investigate this scenario, an additional defect configuration was analysed in which the stress control mastic was removed and an air-filled void was introduced directly underneath the stress control tube approximately 1 mm from the semiconductive screen end. The location of the void was selected based on the most electrically stressed air bubble configuration identified in the previous investigation (Case B1), allowing the influence of the missing stress control mastic to be evaluated under a conservative worst-case condition. This configuration represents a possible assembly error where the stress control tube is shrunk directly onto the underlying insulation without the application of the stress control mastic.

3.3.4 Moisture-Related Defects

Moisture-related defects were introduced into the numerical model in order to investigate the influence of conductive surface contamination on the electric field distribution in the cable termination.
In practical termination assembly process, moisture may trapped between termination layers. The presence of moisture near critical insulation interfaces may distort the local electric field distribution and contribute to partial discharge activity and insulation degradation.
In this study, the moisture defect was modelled as a thin conductive moisture layer positioned on the surface of the XLPE insulation. The moisture layer

was modelled with a thickness of 0.04 mm and a length of 10 mm, extending circumferentially around the insulation surface. The electrical properties assigned to the moisture region were based on the Table 3.2.
Three different moisture configurations were investigated, as illustrated in Figure 3.12.
In configuration (a), the moisture layer was directly connected to the semiconductive screen end. In (b) configuration, the moisture layer was positioned at a distance of 5 mm from the semiconductive screen end, and in (c) configuration, the moisture layer was positioned at a distance of 40 mm from the semiconductive screen end in order to evaluate the influence of the moisture location on the electric field distribution.

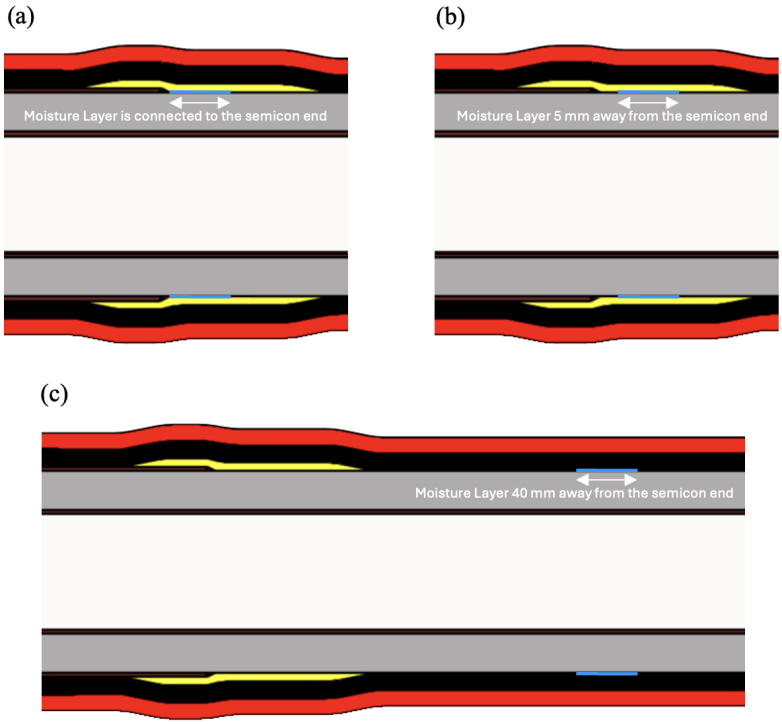

Figure 3.12: Investigated moisture defect configurations represents: (a) connected to the semiconductive screen end, (b) 5 mm away from the semiconductive screen end, and (c) 40 mm away from the semiconductive screen end.

The investigated moisture configurations were selected to represent possible surface moisture contamination occurring near the stress grading region during service conditions.

3.4 Summary of Methodology

This chapter presented the numerical methodologies employed in this thesis for the investigation of electric field behaviour in medium-voltage cable

terminations. A three-dimensional COMSOL model of the investigated cable termination was developed based on manufacturer data, measured dimensions, and material properties obtained from literature and technical documentation. The modelling procedure included geometry development, material assignment, meshing strategy, boundary condition implementation, and solver configuration.
In addition, several defect configurations were introduced into the model in order to investigate the influence of assembly-related imperfections on the electric field distribution. These included air bubble defects, air cushion defects, moisture-related defects, geometrical variations associated with the semiconductive screen end and stress control components.
The simulation results obtained using these methodologies are presented and discussed in Chapter 4.

4

Results and Discussion

4.1 Electric Field Distribution in the Reference Termination

The electric field distribution in the reference termination was first investigated in order to establish the baseline electrical behaviour of the termination under healthy operating conditions. The reference configuration does not contain intentionally introduced air defects, moisture layers, or geometrical imperfections.
Figure 4.1 presents the simulated electric field distribution. The highest electric field concentration was observed in the screen cut-back region. This observation indicates that the electric field is not uniformly distributed throughout the termination structure and that significant field enhancement occurs near the geometrical transition region.

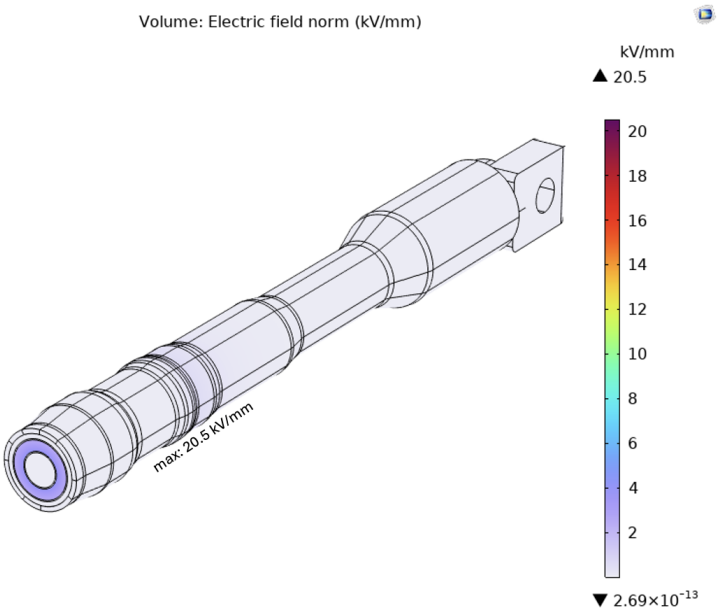

Figure 4.1: Electric field distribution in the reference termination under healthy operating conditions.

In order to more clearly identify the exact location of the maximum electric field, the outer tube, stress control tube, and stress control mastic were hidden from the visualization. The same visualization approach is adopted throughout

the subsequent defect investigations in this chapter to improve the visibility of local electric field concentration regions.
The resulting electric field distribution is presented in Figure 4.2.
The results show that the maximum electric field is concentrated near the end of the semiconductive insulation screen, close to the XLPE insulation surface in the screen cut-back region. The maximum electric field obtained in the reference configuration was approximately 20.5 kV/mm.
Although no defects were present in the reference configuration, the maximum electric field was still concentrated near the semiconductive screen cut-back region. This observation demonstrates that the screen termination itself inherently represents the most critical electrical stress region within the cable termination. The interruption of the coaxial cable geometry at the screen end forces the electric potential to redistribute between the grounded semiconductive screen and the surrounding insulation structure. Consequently, significant electric field enhancement occurs even under healthy operating conditions.
This finding is particularly important because it identifies the screen cut-back region as the location most sensitive to assembly defects. Therefore, the subsequent defect investigations presented in this chapter focus primarily on this region in order to evaluate how different defect types influence the local electric field distribution.

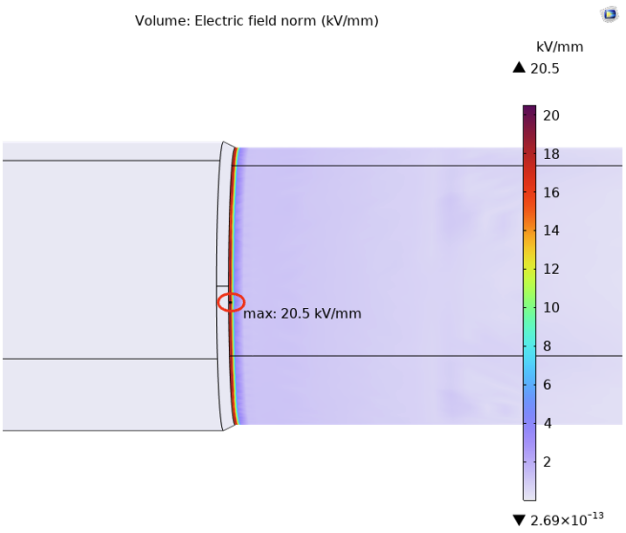

Figure 4.2: Zoomed electric field distribution near the screen cut-back region showing the location of the maximum electric field in the reference termination.

In order to further evaluate the electric field behaviour across the material interfaces, the electric field was extracted along the radial path shown in Figure 4.3 (a). The extraction path starts from the XLPE insulation and extends radially outward through the stress control mastic, stress control tube, and outer tube. The maximum electric field occurs near the screen cut-back region, where the semiconductive insulation screen terminates. Therefore, the extraction path crosses the region where the semiconductive insulation screen is no longer present, resulting in a strong electric field concentration at the

interface between the XLPE insulation and the stress grading materials.

The corresponding radial electric field distribution is presented in Figure 4.3 (b). The results show a significant increase in electric field intensity near the interface between the XLPE insulation and the stress control mastic. After reaching the maximum value in the cut-back region, the electric field decreases rapidly through the stress control materials.

These results confirm that the screen cut-back region represents the most electrically stressed region within the investigated termination structure. This behaviour can be explained by the abrupt geometrical and electrical transition occurring at the semiconductive screen end. According to classical high-voltage field theory, geometrical discontinuities and interfaces between materials with different electrical properties cause compression of the equipotential lines and consequently increase the local electric potential gradient [18]. Since the electric field is directly related to the spatial gradient of the electric potential, the strongest electric field concentration occurs near the screen cut-back region where the equipotential distribution becomes most distorted.

The stress control mastic and stress control tube subsequently redistribute the electric potential and smooth the electric field distribution away from the screen end. This behaviour is reflected in the radial electric field distribution shown in Figure 4.3 (b), where the electric field decreases rapidly after passing through the stress grading materials. Therefore, the screen cut-back region was selected as the primary region of interest for the subsequent defect investigations presented in the following sections.

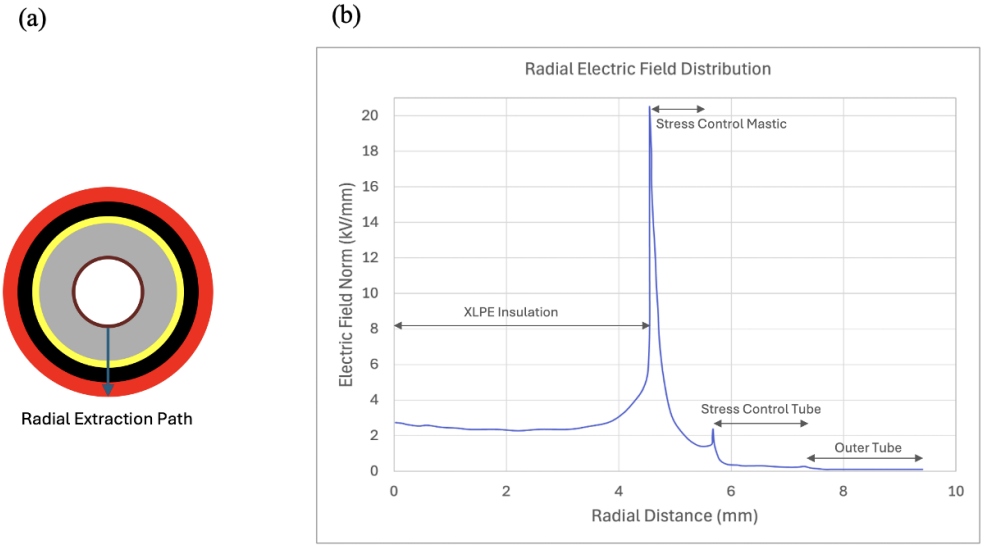

Figure 4.3: Selected radial extraction path used for electric field evaluation in the reference termination (a), and the corresponding radial electric field distribution extracted across the insulation and stress grading layers (b).

4.2 Electric Field Analysis of Defect Configurations

4.2.1 Influence of Semiconductive Screen End Geometry

Figure 4.4 presents the simulated electric field distributions for the investigated transition lengths.

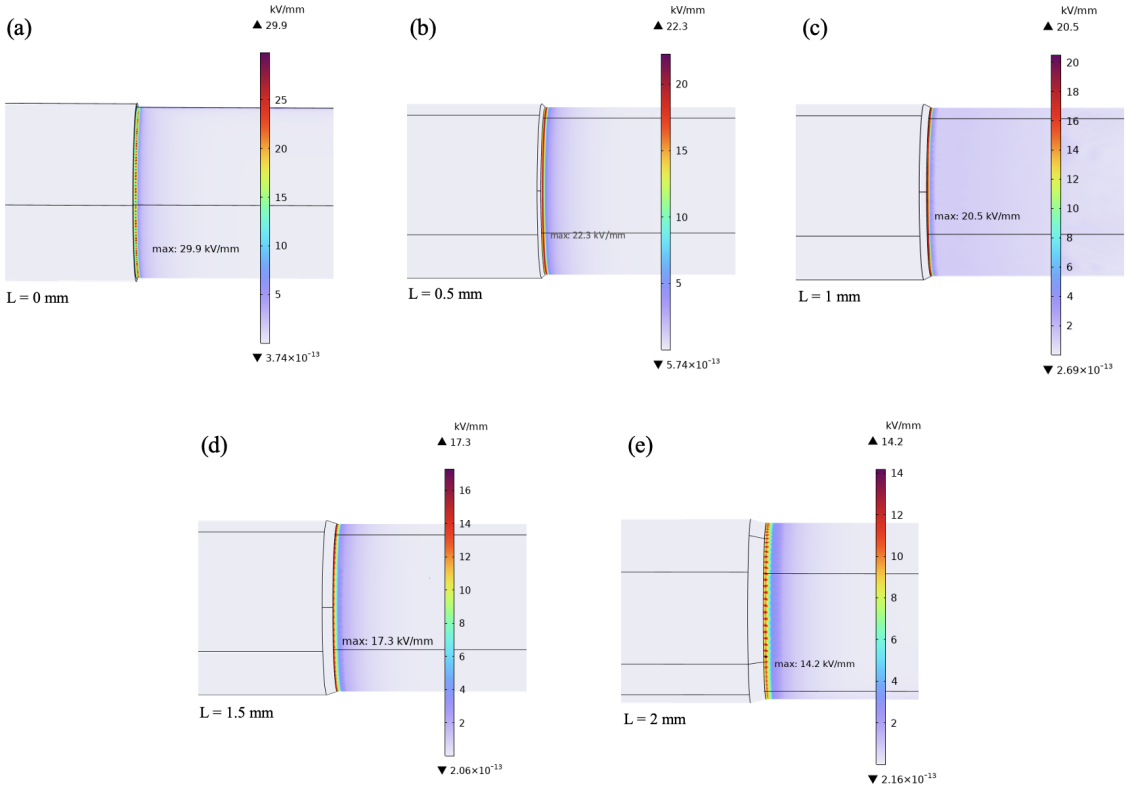

Figure 4.4: Electric field distributions near the semiconductive screen cut-back region for the five different transition lengths L.

The obtained results show that the semiconductive screen end geometry had a significant influence on the electric field distribution. In all investigated configurations, the maximum electric field remained located near the screen cut-back region. However, the magnitude of the maximum electric field changed considerably as the transition length was varied.

For the sharpest configuration, corresponding to $L = 0$ mm, the maximum electric field reached approximately 29.9 kV/mm. In this case, the semiconductive screen terminated abruptly, creating a sharp geometrical discontinuity between the grounded semiconductive screen and the surrounding insulation structure. According to classical high-voltage field theory, abrupt geometrical transitions lead to compression of the equipotential lines and consequently

produce strong electric field concentration [18]. As a result, a pronounced electric field enhancement occurred at the screen cut-back region.

When a short transition length of $L = 0.5$ mm was introduced, the maximum electric field decreased to approximately 22.3 kV/mm. Although the geometrical transition became smoother compared with the sharp edge configuration, the electric potential distribution was still forced to change over a relatively short distance. Consequently, the local electric potential gradient remained high, resulting in elevated electric field levels near the screen end.

The reference configuration, corresponding to $L = 1$ mm, produced a maximum electric field of approximately 20.5 kV/mm. In this configuration, the transition between the semiconductive screen and the surrounding insulation became more gradual, reducing the compression of the equipotential lines and lowering the electric field enhancement at the cut-back region.

Further increasing the transition length continued to reduce the maximum electric field. For $L = 1.5$ mm, the maximum electric field decreased to approximately 17.3 kV/mm, while for $L = 2$ mm the maximum electric field was further reduced to approximately 14.2 kV/mm. These results indicate that extending the transition region allows the electric potential to redistribute more gradually between the grounded semiconductive screen and the surrounding insulation structure. Consequently, the local electric potential gradient becomes smaller, leading to lower electric field concentration near the screen end.

Figure 4.5 summarizes the variation of the maximum electric field as a function of the semiconductive screen transition length.

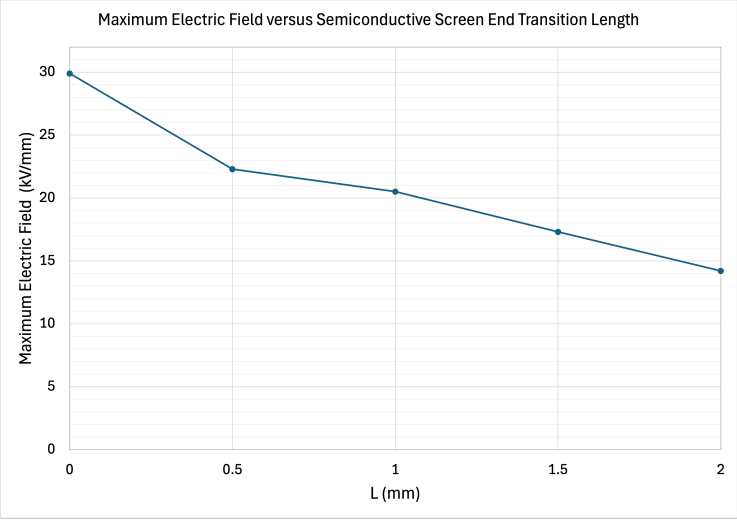

Figure 4.5: Variation of the maximum electric field with semiconductive screen end transition length L.

A clear decreasing trend can be observed as the transition length increases. The maximum electric field decreased from approximately 29.9 kV/mm for

the sharp screen end configuration to approximately 14.2 kV/mm for the smoothest investigated geometry. This corresponds to a reduction of more than 50% in the maximum electric field level.
The obtained results demonstrate that the geometry of the semiconductive screen end is one of the dominant factors governing the electric field distribution in the termination. Smoother screen end transitions promote a more gradual redistribution of the electric potential and reduce local electric field concentration at the cut-back region. Consequently, appropriate shaping of the semiconductive screen end can significantly improve electric field grading performance and reduce the risk of localized electrical overstress within the cable termination structure.

4.2.2 Influence of Stress Control Component Length

Figure 4.6 presents representative electric field distributions for the investigated configurations.

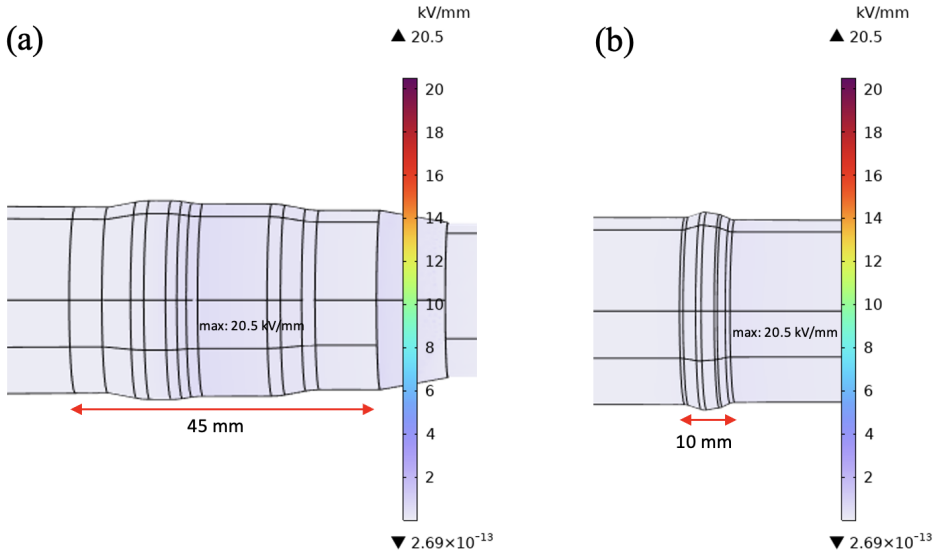

Figure 4.6: Electric field distributions for: (a) reduced stress control tube length and (b) reduced stress control mastic length.

The obtained results show that the investigated reductions in both stress control tube length and stress control mastic length had a negligible influence on the overall electric field distribution within the cable termination. In all investigated configurations, the maximum electric field remained approximately 20.5 kV/mm, corresponding to the reference termination.

Furthermore, the location of the maximum electric field remained unchanged and continued to occur near the semiconductive screen cut-back region. This observation indicates that the electric field distribution was primarily governed by the local geometry of the screen end and the associated stress grading region rather than by the investigated reductions in the axial lengths of the

surrounding stress control components.

For the reduced stress control tube configuration, the electric field distribution remained almost identical to the reference case. Although the stress control tube length was reduced, the critical screen cut-back region remained fully covered by the stress grading materials. Consequently, the surrounding equipotential distribution and electric field grading mechanism were preserved, preventing any significant increase in electric field concentration.

A similar behaviour was observed for the reduced stress control mastic configuration. Despite the shorter mastic length, the stress control material continued to cover the electrically critical region surrounding the semiconductive screen end. As a result, the electric potential gradient in the cut-back region remained largely unchanged, and no noticeable increase in electric field enhancement was observed.

These results indicate that moderate reductions in the investigated stress control component lengths do not necessarily lead to deterioration of the electric field distribution. The effectiveness of the stress grading system appears to depend primarily on maintaining adequate coverage of the semiconductive screen cut-back region rather than on the total axial length of the stress control components.
Therefore, under the investigated geometrical conditions, the stress grading mechanism remained effective even after the reduction of the stress control tube and stress control mastic lengths. As long as the critical screen cut-back region remains sufficiently covered by the stress grading materials, only minor changes in the electric field distribution are expected.

4.2.3 Influence of Air Defects

4.2.3.1 Air Bubble Defects

Figure 4.7 presents the simulated electric field distributions for the investigated air bubble configurations.
The obtained results show that localized air bubble defects may significantly increase the electric field inside the cable termination compared with the reference configuration, where the maximum electric field was approximately 20.5 kV/mm. The highest electric field enhancement was obtained for Case B1, where the maximum electric field in the overall termination reached approximately 60.4 kV/mm. The remaining bubble configurations produced lower, but still elevated, maximum electric field values of 35.0 kV/mm, 30.7 kV/mm, and 21.6 kV/mm for Cases B2, B3, and B4, respectively.

In Case B1, the air bubble was positioned mainly along the XLPE insulation surface approximately 1 mm away from the semiconductive screen end. In this region, the electric field is naturally concentrated due to the interruption of the coaxial cable geometry at the screen cut-back region. Since air

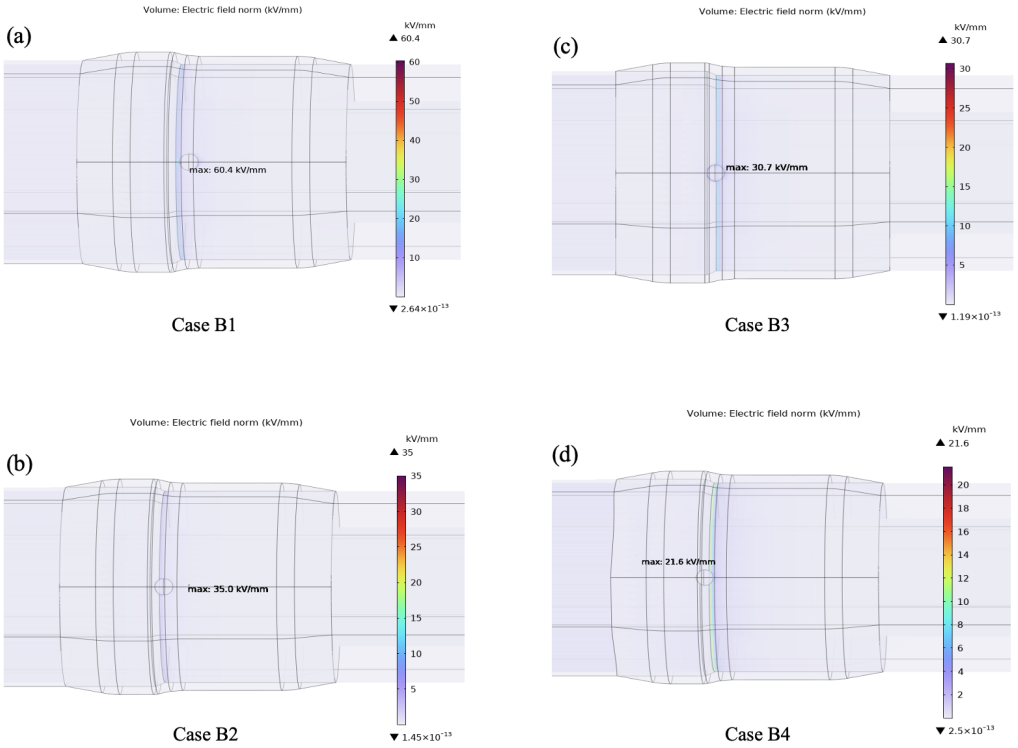

Figure 4.7: Electric field distributions for the four investigated air bubble defect cases under the stress control mastic.

has a significantly lower relative permittivity than XLPE insulation, the air bubble introduced a strong dielectric discontinuity directly inside the critical stress region. According to classical high-voltage field theory, electric field enhancement commonly occurs at interfaces between materials with different dielectric permittivities and at geometrical discontinuities where the equipotential distribution becomes distorted [18]. Consequently, substantial electric field crowding occurred around the bubble boundaries, resulting in the highest electric field enhancement among the investigated air bubble cases.

In Case B2, the air bubble was shifted closer to the sloped semiconductive screen cut-back region, where the beginning of the bubble was positioned approximately at the middle of the semiconductive screen slope. Compared with Case B1, the maximum electric field in the overall termination decreased to approximately 35.0 kV/mm. This reduction can be attributed to the increased influence of the semiconductive screen region, which partially redistributed the local electric stress and reduced the field enhancement in the surrounding insulation region.

However, despite the lower overall electric field in the termination, Case B2 produced the highest electric field inside the air-filled cavity itself, reaching approximately 28.2 kV/mm. This behaviour indicates that the electric field inside the cavity did not directly follow the same trend as the maximum electric field in the overall termination. In this configuration, the local equipotential

distribution around the cavity caused stronger penetration of electric field lines through the air region itself, producing highly concentrated electric stress inside the cavity volume.

In Case B3, the air bubble was positioned closer to the beginning of the semiconductive screen slope. In this region, the stress grading effect of the semiconductive screen and stress control materials became more effective in redistributing the local electric field. Consequently, the maximum electric field in the termination decreased further to approximately 30.7 kV/mm. Nevertheless, the air cavity still produced considerable local electric field enhancement due to the dielectric discontinuity introduced by the low-permittivity air region embedded inside the insulation structure.

In Case B4, the air bubble was positioned such that most of the cavity was in contact with the semiconductive screen region. In this configuration, the semiconductive screen had the strongest shielding influence on the local electric field distribution. Since the semiconductive screen is maintained close to ground potential, the surrounding equipotential lines became more uniformly distributed around the cavity region, reducing the electric field enhancement in the overall termination. As a result, the maximum electric field decreased to approximately 21.6 kV/mm, which was close to the reference value.

Despite the lower overall electric field in Case B4, the electric field inside the cavity itself remained relatively high at approximately 22.8 kV/mm. This behaviour can be explained by the strong dielectric mismatch between air and the surrounding insulation materials. Even when the overall field distribution is partially suppressed by the semiconductive screen, localized electric field enhancement may still occur inside the cavity due to the concentration of electric flux at the air-solid interfaces.

Table 4.1 summarizes the maximum electric field values both in the overall termination and inside the air-filled cavities.

Table 4.1: Maximum electric field values for the investigated air bubble configurations.

Case	Maximum field in overall termination (kV/mm)	Maximum field inside air bubble (kV/mm)
B1	60.4	11.7
B2	35.0	28.2
B3	30.7	16.7
B4	21.6	22.8

In addition to the magnitude, the location of the maximum electric field in the termination also varied among the investigated cases. For Cases B1 and B2, the maximum field remained concentrated near the screen cut-back region and the bubble boundaries, whereas in Cases B3 and B4 the maximum field shifted

closer to the semiconductive screen interface due to the increased influence of the grounded semiconductive layer.

Figure 4.8 illustrates the electric field distributions inside the investigated air bubble defects. The results show that both the magnitude and location of the maximum electric field inside the cavities varied considerably between the investigated cases, indicating that the local cavity field strongly depends on the cavity position, surrounding material interfaces, and local equipotential distribution.
For visualization purposes, the air bubble geometries shown in Figure 4.8 were rotated in order to clearly illustrate the locations of the maximum electric field regions inside the investigated cavities.

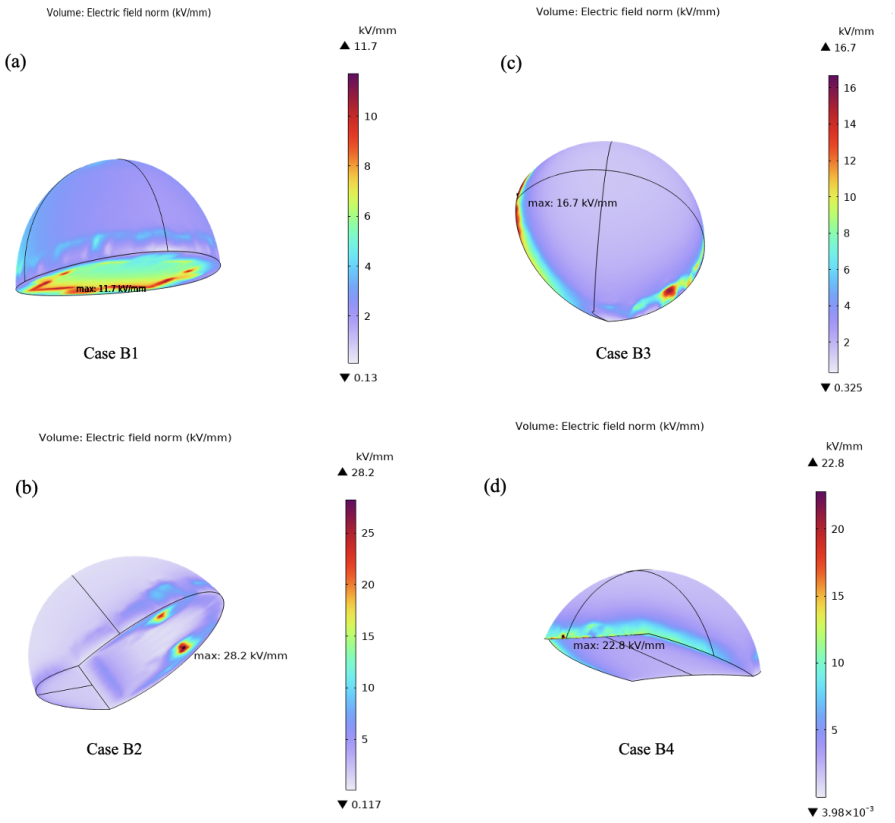

Figure 4.8: Electric field distributions inside the four investigated air bubble defect cases under the stress control mastic.

For reference, the commonly cited breakdown strength of air under uniform field conditions is approximately 3 kV/mm [18]. Although partial discharge inception may occur at lower electric field levels depending on cavity geometry, pressure, and field non-uniformity, this value provides a useful reference for evaluating the severity of the investigated air-filled defects.
Among the investigated air bubble cases, the electric field inside the air bubble reached values between 11.7 kV/mm and 28.2 kV/mm. These values are

considerably higher than the breakdown strength of air. Furthermore, partial discharge inception inside gaseous cavities may occur at electric field levels lower than the breakdown strength of air depending on the cavity geometry, pressure, gas composition, and local electric field non-uniformity.

Overall, the results indicate that localized air bubble defects near the semiconductive screen cut-back region may create highly critical electric stress concentrations inside cable terminations. In particular, air bubbles positioned near the XLPE insulation surface and stress grading region may act as favourable sites for partial discharge initiation and progressive insulation degradation. Repeated partial discharge activity inside such cavities may gradually erode the surrounding insulation material and contribute to long-term insulation degradation.

4.2.3.2 Air Cushion Defects

Figure 4.9 presents the simulated electric field distributions for the investigated air cushion configurations.

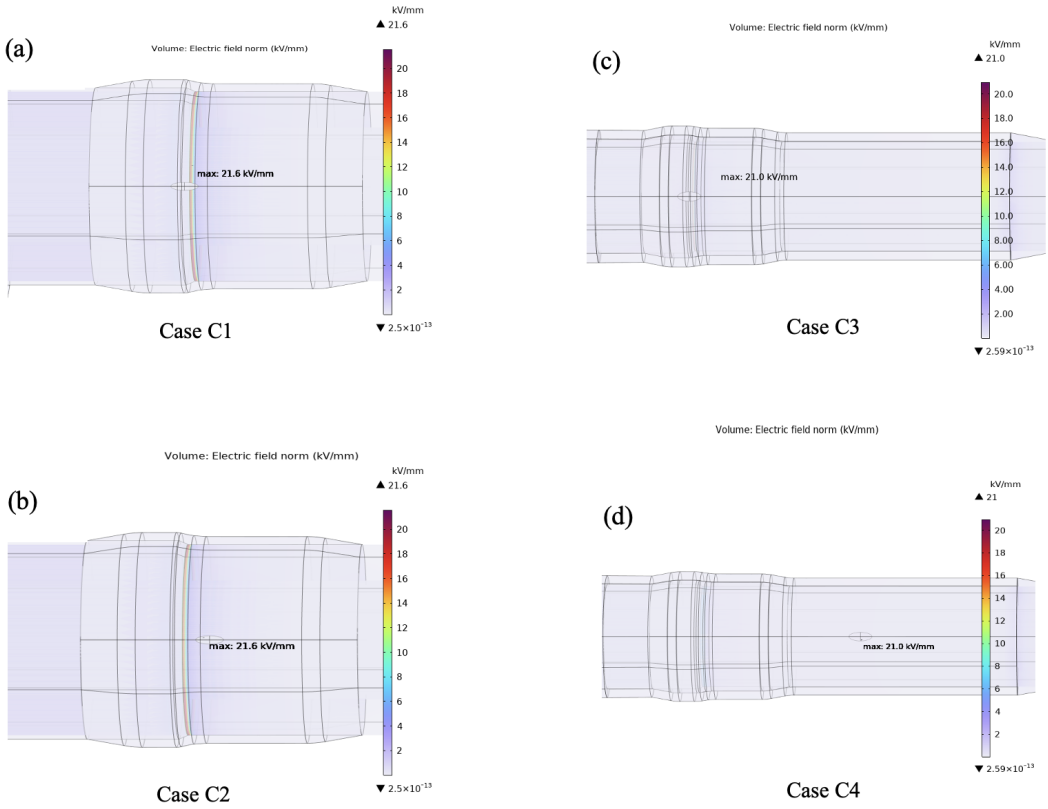

Figure 4.9: Electric field distributions for the investigated air cushion defect cases: (a and b) inside the stress control mastic and (c and d) inside the stress control tube.

The results show that the investigated air cushion defects had only a negligible influence on the overall electric field distribution within the cable termination. The maximum electric field in the termination remained close to the reference value of 20.5 kV/mm, reaching approximately 20.6 kV/mm for Cases C1 and C2 and 20.5 kV/mm for Cases C3 and C4. These results indicate that the presence of the investigated air cushions did not significantly modify the global electric stress distribution within the termination structure.
Although the overall electric field distribution remained largely unaffected, the electric field inside the air-filled regions varied considerably depending on the location of the air cushion within the stress grading structure. Figure 4.10 illustrates the electric field distributions inside the investigated air cushion defects, while Table 4.2 summarizes the maximum electric field values obtained inside the cavities.

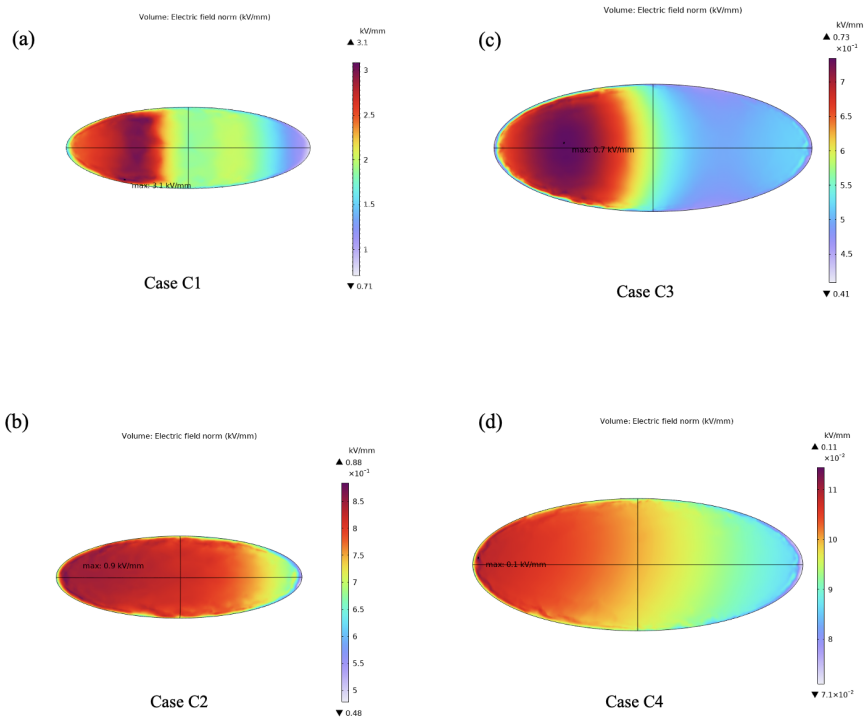

Figure 4.10: Electric field distributions inside the four investigated air cushion defect cases: (a and b) located within the stress control mastic and (c and d) within the stress control tube regions.

Among the investigated cases, the highest electric field inside the air cushion was obtained for Case C1, where the maximum field reached approximately 3.1 kV/mm. In this configuration, the air cushion was located inside the stress control mastic relatively close to the semiconductive screen cut-back region. As demonstrated previously in the reference termination, the cut-back region represents the most electrically stressed part of the termination due to the transition between the grounded semiconductive screen and the surrounding

Table 4.2: Maximum electric field values for the investigated air cushion configurations.

Case	Maximum field in termination (kV/mm)	Maximum field inside air cushion (kV/mm)
C1	20.6	3.1
C2	20.6	0.9
C3	20.5	0.7
C4	20.5	0.1

insulation structure. Consequently, the local electric potential gradient remained relatively high in this region. Since the electric field is directly related to the spatial gradient of the electric potential, the stronger potential gradient surrounding the air cushion resulted in higher electric field levels inside the trapped air region.

For Case C2, the maximum electric field inside the air cushion decreased significantly to approximately 0.9 kV/mm, despite the defect remaining inside the stress control mastic. This result indicates that even relatively small positional changes inside the stress grading region can substantially influence the local electric field conditions. Compared with Case C1, the surrounding electric potential distribution became more gradual, reducing the local potential gradient around the air inclusion and consequently lowering the electric field inside the cavity.

Cases C3 and C4 were located inside the stress control tube region, where the electric field inside the air cushions decreased further to approximately 0.7 kV/mm and 0.1 kV/mm, respectively. These results can be explained by the stress grading function of the surrounding stress control tube material. The purpose of the stress control tube is to smooth the electric potential distribution and reduce electric field gradients along the termination surface. Consequently, the surrounding equipotential lines became more uniformly distributed, producing substantially lower potential gradients around the air inclusions.
The very low electric field observed in Case C4 indicates that the surrounding potential distribution in this region was highly uniform. As a result, only minimal electric field distortion occurred around the air cushion despite the presence of the dielectric discontinuity introduced by the trapped air region.

The obtained results demonstrate that the local electric potential gradient surrounding the air inclusion plays a more important role than the mere presence of the air cushion itself. Air cushions located in regions with stronger potential gradients experienced higher electric field levels, whereas cushions positioned in regions with smoother potential distributions remained exposed to only minor electric stresses.

The electric field obtained inside the air cushion for Case C1 was close to the breakdown strength of air. Consequently, the investigated air cushion located closest to the semiconductive screen cut-back region may represent a potential weak point within the insulation system, where partial discharge inception could occur under sufficiently adverse operating conditions.
In contrast, the remaining air cushion configurations produced considerably lower electric field levels inside the cavities, indicating a substantially lower likelihood of discharge activity under the investigated conditions.
Overall, the results indicate that the severity of air cushion defects depends primarily on their position relative to the local electric potential gradient within the stress grading structure. Air cushions located near regions of stronger potential variation may experience moderate electric field enhancement, whereas similar defects located within more uniform stress grading regions have only a minor influence on the local electrical stress distribution.

4.2.3.3 Comparison of Investigated Air Defects

A comparison of all investigated air defect configurations is presented in Table 4.3. The comparison includes both the maximum electric field in the overall termination and the maximum electric field inside the air-filled defect region.

Table 4.3: Comparison of maximum electric field values for all investigated air defect configurations.

Defect case	Maximum field in termination (kV/mm)	Maximum field inside defect (kV/mm)
B1	60.4	11.7
B2	35.0	28.2
B3	30.7	16.7
B4	21.6	22.8
C1	20.6	3.1
C2	20.6	0.9
C3	20.5	0.7
C4	20.5	0.1
Reference	20.5	–

The results demonstrate that the severity of air defects depends strongly on both the defect geometry and its location within the termination structure. The investigated air bubble defects produced substantially higher electric field enhancement than the air cushion defects, both in the overall termination and inside the air-filled cavities.

In particular, Cases B1–B3 generated significant electric field concentrations near the semiconductive screen cut-back region, while the air cushions had only a minor influence on the overall electric field distribution.

From a partial discharge perspective, the electric field inside the defect is of particular importance. The electric field inside the investigated air bubbles ranged from 11.7 kV/mm to 28.2 kV/mm, significantly exceeding the commonly referenced breakdown strength of air. In contrast, the air cushion defects produced considerably lower cavity field levels, ranging from 0.1 kV/mm to 3.1 kV/mm. These results indicate that localized air bubbles represent the most critical air-related defect configuration among the investigated cases, whereas air cushions located within the stress grading materials appear considerably less severe under the investigated conditions.

4.2.4 Effect of Missing Stress Control Mastic

Figure 4.11 presents the simulated electric field distribution for the investigated configuration.

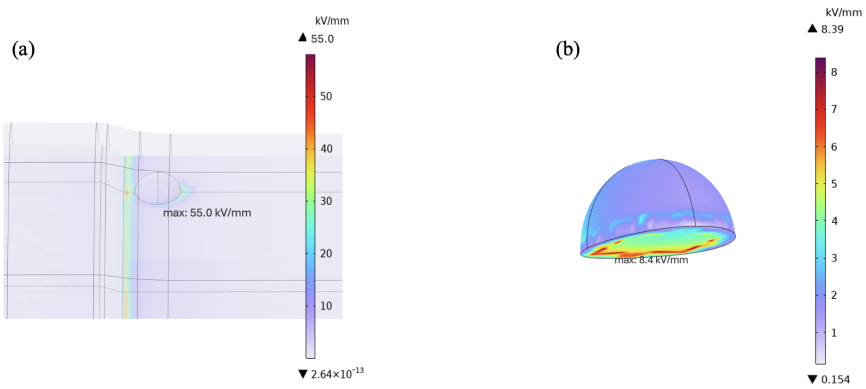

Figure 4.11: Electric field distribution for: (a) an air bubble located directly underneath the stress control tube in the absence of stress control mastic and (b) inside the bubble.

The simulation results showed that the maximum electric field in the overall termination reached approximately 55.0 kV/mm, while the maximum electric field inside the air bubble reached approximately 8.4 kV/mm. These values are significantly higher than those obtained for the reference termination, indicating substantial local electric field enhancement caused by the trapped air region.

Compared with the corresponding air bubble configuration located underneath the stress control mastic, where the maximum electric field in the termination and inside the cavity reached approximately 60.4 kV/mm and 11.7 kV/mm, respectively, a moderate reduction in electric field enhancement was observed. This behaviour can be explained by the electrical properties of the surrounding stress grading materials. In the present configuration, the air bubble was directly adjacent to the stress control tube, which possesses relative permittivity of $\varepsilon_r = 35$ that is higher than the relative permittivity of stress control mastic $\varepsilon_r = 15$. Consequently, the electric potential distribution around the cavity became smoother, resulting in a lower local potential gradient and therefore

lower electric field levels both inside the cavity and within the surrounding insulation.

Although the electric field enhancement was reduced compared with the corresponding bubble located underneath the stress control mastic, the obtained field levels remained significantly elevated. In particular, the electric field inside the air-filled cavity substantially exceeded the commonly referenced breakdown strength of air under uniform field conditions. Therefore, the investigated configuration may still provide favourable conditions for partial discharge initiation and long-term insulation degradation.

The results demonstrate that omission of the stress control mastic during termination assembly may create electrically critical voids within the termination structure. The stress control mastic serves several important functions within the cable termination system. Besides contributing to the electric field grading mechanism, it fills geometrical irregularities and small air gaps that may remain between the cable insulation and the surrounding stress control components during assembly process. By eliminating trapped air pockets and ensuring intimate contact between adjacent materials, the mastic helps maintain a continuous electric potential distribution across the stress grading region. If the mastic is omitted, voids may remain inside the termination structure and act as low-permittivity regions embedded within the insulation system.
According to classical high-voltage field theory, such dielectric discontinuities distort the local equipotential distribution and may lead to localized electric field enhancement at the air-solid interfaces. Therefore, the absence of the stress control mastic not only reduces the effectiveness of the stress grading system but also increases the probability of defect formation capable of initiating partial discharge activity and long-term insulation degradation. Consequently, correct application of the stress control mastic remains essential for ensuring reliable electric field grading and minimizing the risk of defect-induced electrical overstress.

4.2.5 Moisture Defect

Figure 4.12 presents the simulated electric field distributions for the investigated moisture defect configurations.
The results show that the presence and position of the moisture layer influenced the electric field distribution.

When the moisture layer was directly connected to the semiconductive screen, Figure 4.12 (a), the maximum electric field in the termination reached approximately 26.7 kV/mm. In this configuration, the electric field enhancement mainly appeared near the edge of the moisture layer at its interface with the XLPE insulation and stress control mastic.
This behaviour can be explained by the conductive nature of the moisture layer and its electrical connection to the semiconductive screen. Since the

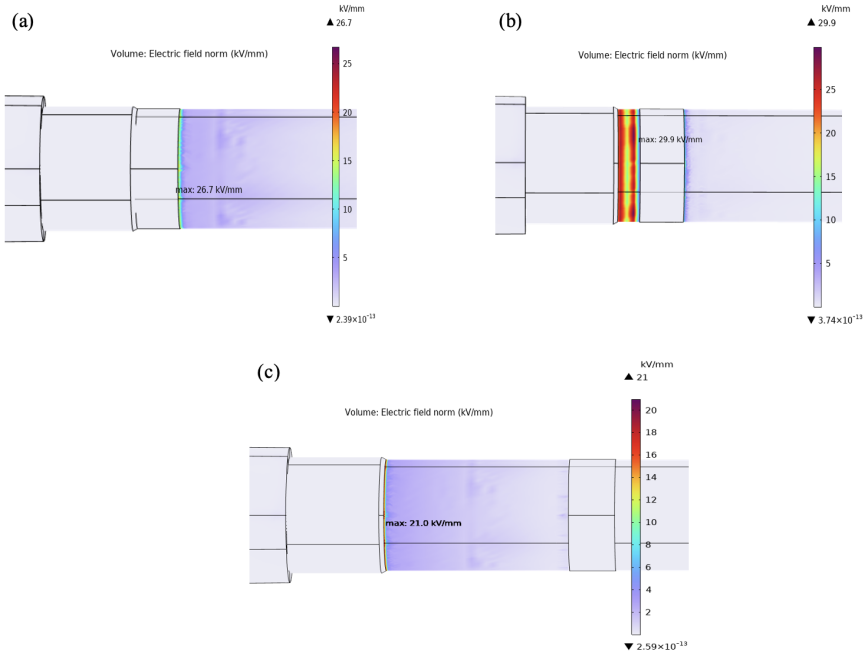

Figure 4.12: Electric field distributions when the moisture layer is: (a) connected to the semiconductive screen end, (b) floating layer located 5 mm away from the semiconductive screen end, (c) floating layer located 40 mm away from the semiconductive screen end configurations.

semiconductive screen is maintained ground potential, the connected moisture layer also tends to assume nearly the same electrical potential. As a result, the moisture region behaves as an extension of the grounded semiconductive screen, which modifies the local equipotential distribution near the screen cut-back region. Consequently, the electric field becomes concentrated at the outer edge of the moisture layer, where the grounded conductive region terminates and transitions towards the surrounding dielectric materials.

When the moisture layer was positioned 5 mm away from the semiconductive screen end and underneath the stress control mastic region, Figure 4.12 (b), the maximum electric field increased further to approximately 29.9 kV/mm. In this configuration, the moisture region behaved as a floating conductive layer since it was not electrically connected to either the semiconductive screen or any grounded component. As a result, the electric field became strongly concentrated around the floating moisture region itself, producing a more localized field enhancement compared with the connected moisture configuration.

This behaviour can be explained by the electrical properties of moisture contamination. In the present simulations, the moisture layer was assigned a relative permittivity of $\varepsilon_r = 80$ and an electrical conductivity of $\sigma = 10^{-2}$ S/m, representing conductive moisture contamination compared with the surrounding XLPE insulation. Due to the presence of dissolved ions and increased conductivity compared with the surrounding polymer insulation materials, mois-

ture regions can behave as partially conductive inclusions within the insulation system. According to classical high-voltage field theory, conductive inclusions embedded inside dielectric materials distort the local equipotential distribution and produce electric field enhancement at their boundaries, particularly at regions with abrupt conductivity transitions [18].
In the present case, the floating moisture layer introduced an isolated conductive discontinuity inside the stress grading region. Although the moisture layer was not electrically connected to the conductor, the simulation results showed that the floating moisture region assumed an electric potential close to the conductor potential due to capacitive coupling and charge redistribution within the conductive moisture layer. Consequently, a strong potential gradient was formed between the grounded semiconductive screen and the floating high-potential moisture region.
This large potential difference over a relatively short distance produced significant electric field crowding around the boundaries of the moisture layer, leading to stronger local electric field enhancement compared with the moisture configuration connected to the semiconductive screen.

Figure 4.13 illustrates the corresponding electric potential distributions for the investigated floating moisture configurations.

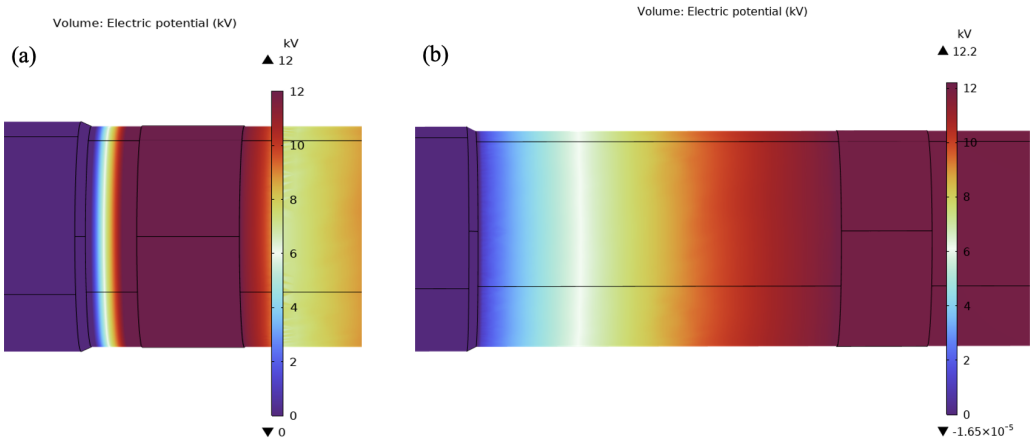

Figure 4.13: Electric potential distributions for the investigated floating moisture defect located: (a) 5 mm away from the semiconductive screen end and (b) 40 mm away from the semiconductive screen end configurations.

When the moisture layer was positioned further away from the semiconductive screen end and underneath the stress control tube region, Figure 4.12 (c), the electric field distribution remained close to the reference configuration approximately 21.0 kV/mm. In this case, the maximum electric field in the termination was only slightly different from the reference value, indicating that the investigated moisture defect had a limited influence on the overall stress distribution when located far from the semiconductive screen cut-back region. Compared with the floating moisture defect located near the semiconductive screen end, the electric field enhancement around the moisture region was sig-

nificantly reduced. This behaviour can be explained by the local electric field conditions inside the stress grading region. The highest electric field gradients in cable terminations are typically concentrated near the semiconductive screen cut-back area due to the abrupt geometrical and electrical discontinuity between the grounded semiconductive screen and the insulation region. When the moisture layer was moved further away from this critical region, the surrounding electric field became more uniform, resulting in weaker field distortion around the conductive moisture inclusion.

Although the moisture layer still behaved as a floating conductive region due to its finite conductivity, the potential difference between the moisture layer and the surrounding insulation structure was lower compared with the previous floating moisture configuration near the cut-back region. Consequently, the electric field crowding at the moisture boundaries was reduced, leading to a lower local electric field enhancement.

These results indicate that the position of conductive moisture contamination plays an important role in determining its influence on the electric field distribution. Moisture defects located close to the semiconductive screen cut-back region may produce significant local electric field enhancement, whereas similar defects positioned further inside the stress control tube region have a considerably smaller impact on the electrical stress distribution.

Table 4.4: Maximum electric field values for the investigated moisture defect configurations.

Moisture defect configuration	Maximum electric field (kV/mm)
Moisture layer connected to semicon	26.7
Moisture layer 5 mm away from semicon	29.9
Moisture layer 40 mm away from semicon	21.0
Reference case	20.5

Overall, the results demonstrate that the influence of moisture contamination strongly depends on its position relative to the semiconductive screen cut-back region. As shown in Table 4.4, The most critical configuration was the floating moisture layer located close to the semiconductive screen end, which produced the highest electric field enhancement due to the strong local potential gradient formed between the grounded semiconductive screen and the floating conductive moisture region. In contrast, the moisture defect located further underneath the stress control tube produced only minor distortion of the electric field distribution because of the more uniform potential distribution inside the stress grading region.

These results indicate that conductive moisture contamination near the screen cut-back region may significantly increase the risk of local electrical overstress and partial discharge activity in cable termination systems.

4.3 Chapter Summary

This chapter presented the simulation results obtained for the investigated medium-voltage cable termination and evaluated the influence of geometrical variations, assembly-related imperfections, air-filled defects, and moisture contamination on the electric field distribution.

The reference configuration demonstrated that the highest electric field concentration occurs at the semiconductive screen cut-back region, confirming that this area represents the most electrically stressed part of the termination.

The results further showed that the geometry of the semiconductive screen end has a significant influence on the electric field distribution. Increasing the transition length at the screen cut-back reduced the maximum electric field, indicating that smoother geometrical transitions improve electric field grading and reduce local field enhancement.

In contrast, the investigated reductions in stress control tube and stress control mastic lengths produced only minor changes in the maximum electric field. As long as the critical screen cut-back region remained adequately covered by the stress grading materials, the overall electric field distribution was largely preserved.

Among the investigated defect types, localized air bubble defects produced the most severe electric field enhancement. The magnitude of the electric field was strongly dependent on the bubble position and its contact with surrounding materials. Several air bubble configurations generated electric field levels inside the cavity that substantially exceeded the breakdown strength of air, indicating favourable conditions for partial discharge inception. Air cushion defects exhibited a significantly lower influence on both the overall electric field distribution and the electric field inside the defect region. The results showed that both the geometry and location of trapped air regions play important roles in determining their electrical severity.

The investigated missing-mastic configuration demonstrated that omission of the stress control mastic may allow air-filled voids to remain inside the termination structure, resulting in elevated local electric field levels. This finding highlights the importance of proper assembly practices and correct application of stress control materials.

The moisture defect investigation showed that conductive moisture contamination can significantly affect the local electric field distribution. Moisture layers connected to the semiconductive screen modified the local field distribution near the screen cut-back region, while floating moisture layers produced stronger local electric field enhancement due to conductive inclusion effects and local potential redistribution. The severity of the moisture defect was found to depend strongly on its position relative to the semiconductive screen end and the stress grading region.

Overall, the results demonstrate that the electrical performance of medium-voltage cable terminations is governed not only by the intended stress grading design but also by assembly quality, material interfaces, and defect characteristics. Defects located near the semiconductive screen cut-back region were con-

sistently found to produce the highest electric field enhancement and therefore represent the most critical locations from an insulation reliability perspective.

5
Conclusion

This thesis investigated the electric field distribution in a medium-voltage cable termination and evaluated the influence of assembly-related defects and geometrical variations using three-dimensional finite element simulations in COMSOL Multiphysics.

A reference termination model was first developed to establish the baseline electric field distribution under healthy operating conditions. The results demonstrated that the highest electric field concentration occurs near the semiconductive screen cut-back region, confirming that this area represents the most electrically stressed part of the termination structure. Consequently, the screen cut-back region was identified as the most critical location for defect-related electric field enhancement.

The influence of the semiconductive screen end geometry was investigated by varying the transition length at the screen cut-back. The results showed that smoother transitions significantly reduce the maximum electric field, whereas sharp semiconductive screen edges produce substantial electric field concentration. These findings highlight the importance of proper screen preparation and geometrical design for effective electric field control.

The influence of stress grading component dimensions was also evaluated. The investigated reductions in the lengths of the stress control tube and stress control mastic produced no measurable change in the maximum electric field, which remained identical to the reference configuration. This indicates that the electric field grading performance is primarily governed by the coverage of the screen cut-back region rather than by the investigated reductions in the axial lengths of the stress grading components. As long as the critical cut-back region remained adequately covered by the stress grading materials, the overall electric field grading performance was largely preserved.

Several air-related defects were investigated, including air bubbles, air cushions, and a missing stress control mastic scenario. Among the analysed air defects, localized air bubbles located near the semiconductive screen cut-back region produced the highest electric field enhancement. The results demonstrated that defect position and interaction with surrounding material interfaces strongly influence both the electric field inside the cavity and the maximum electric field within the termination. In contrast, air cushion defects produced considerably smaller electric field enhancement in the overall termination and inside the air cushions as well, particularly when located inside the stress control tube. The missing stress control mastic scenario further demonstrated the importance of proper assembly practices, as omission of the mastic

may create conditions that allow electrically critical air-filled voids to remain trapped within the termination structure.
Moisture-related defects were also found to influence the electric field distribution significantly. The results showed that floating moisture layers located near the semiconductive screen cut-back region produced stronger electric field enhancement than moisture layers electrically connected to the semiconductive screen. In contrast, moisture contamination positioned further away from the cut-back region had only a limited influence on the overall electric field distribution. These findings demonstrate that both the electrical behaviour and the location of moisture contamination are important factors governing its impact on insulation performance.
Overall, the results demonstrate that the electrical performance of medium-voltage cable terminations is highly dependent on both termination geometry and assembly quality. Defects located close to the semiconductive screen cut-back region were consistently found to produce the largest electric field enhancement and therefore represent the most critical locations from an insulation reliability perspective. The findings contribute to an improved understanding of defect-induced electric field distortion in cable terminations and may support improved termination design, installation practices, condition assessment, and reliability evaluation of medium-voltage cable accessories.

5.1 Future Work

The present work focused on electric field analysis of medium-voltage cable terminations under healthy and defective installation conditions using finite element simulations. Although the obtained results provide valuable insight into defect-induced electric field enhancement, several aspects remain suitable for further investigation.

Future studies may investigate a wider range of defect geometries, dimensions, and locations. In practical installations, defects rarely occur in idealized shapes and may exhibit irregular geometries, non-uniform distributions, and varying material properties. Furthermore, the interaction between multiple defects may influence the electric field distribution and assembly performance differently from isolated defects.
The present study considered a single-phase termination model. Future work could investigate the interaction between adjacent phases in a complete three-phase termination assembly. Such analyses may provide additional insight into phase-to-phase electric field interactions and their influence on local stress concentrations, particularly in regions where the phases are brought into close proximity.

Bibliography

[1] M. Pompili, L. Calcara, L. D'Orazio, D. Ricci, A. Derviškadić, and H. He, *Joint defectiveness of MV underground cable and the effects on the distribution system*, Electric Power Systems Research, vol. 192, 107004, 2021.

[2] X. Xu, *Power Cable Diagnostic Review*, Energiforsk Report 2022:903, Sweden, 2022.

[3] Z. A. Tamus, B. Nemeth, I. Kiss, R. Cselko, I. Berta, *Complex Examination of a Cable Terminal Failure*, IEEE Conference Paper, 2008.

[4] A. Suhaimi and H. S. A. Halim, *Failure Analysis of Cable Accessories Using Finite Element Method Magnetics (FEMM) Software*, IEEE Conference on Condition Monitoring and Diagnosis, 2012.

[5] O. Kuusisto, *The Effects of Installation-Based Defects in Medium Voltage Cable Joints*, Bachelor's Thesis, Helsinki Metropolia University of Applied Sciences, 2016.

[6] NKT Cables, *Kraftkabelhandboken*, NKT Cables AB, Sweden, 2015.

[7] A. F. Andrade, E. G. Costa, F. L. M. Andrade, C. S. H. Soares, and G. R. S. Lira, "Design of Cable Termination for AC Breakdown Voltage Tests," *Energies*, vol. 12, no. 16, p. 3075, 2019.

[8] G. F. Moore, *Electric Cables Handbook*, 3rd ed., Blackwell Science Ltd., Oxford, United Kingdom, 1997.

[9] J. C. Fothergill and R. N. Hampton, "Polymer Insulated Power Cables," in *Advances in High Voltage Engineering*, A. Haddad and D. Warne, Eds., The Institution of Engineering and Technology, Stevenage, United Kingdom, 2004, pp. 477–510.

[10] Riyadh Cables, *Medium Voltage Cables (MV)*, Available: `https://riyadh-cables.com/product-category/medium-voltage-cables-mv/`, Accessed: June 2026.

[11] IEEE, *IEEE Recommended Practice for Installation, Termination, and Testing of Insulated Power Cable as Used in Industrial and Commercial Applications*, IEEE Std 576-2000, IEEE, New York, USA, 2000.

[12] Ensto, *Installation Instruction HIT3.2413L Heat Shrink Termination*, 2019.

[13] Ensto, *Solutions for Underground Cable Networks 1–42 kV*, 2024.

[14] Nexans, *Medium Voltage Cable Accessories Catalogue*, Nexans Power Accessories, France, 2020.

[15] M. N. O. Sadiku, *Elements of Electromagnetics*, 7th ed., Oxford University Press, New York, USA, 2018.

[16] E. Kuffel, W. S. Zaengl, and J. Kuffel, *High Voltage Engineering Fundamentals*, 2nd ed., Butterworth-Heinemann, Oxford, United Kingdom, 2000.

[17] D. J. Griffiths, *Introduction to Electrodynamics*, 4th ed., Cambridge University Press, Cambridge, United Kingdom, 2013.

[18] A. Küchler, *High Voltage Engineering: Fundamentals, Technology and Applications*, Springer Vieweg, Berlin, Germany, 2018.

[19] S. Christou, *Thermal Prognostic Condition Monitoring for MV Cable Systems*, PhD Thesis, University of Southampton, Faculty of Physical Sciences and Engineering, Department of Electronics and Computer Science, 2016.

[20] J. Densley, *Ageing Mechanisms and Diagnostics for Power Cables—An Overview*, IEEE Electrical Insulation Magazine, vol. 17, no. 1, pp. 14–22, 2001.

[21] C. C. Uydur and O. Arikan, *Use of Tanδ and Partial Discharge for Evaluating the Cable Termination Assembly*, Energies, vol. 13, no. 20, 5299, 2020.

[22] M. Pompili and L. Calcara, *Qualification of MV Cable Joints: Partial Discharges Innovative Tests*, IEEE International Conference on Environment and Electrical Engineering (EEEIC), 2024.

[23] C. Suwanasi, T. Suwanasri, P. Fuangpian, and S. Ruankon, *Investigation on Partial Discharge of Power Cable Termination Defects Using High Frequency Current Transformer*, IEEE Conference Paper, 2013.

[24] D. Xin, G. Wu, G. Gao, K. Chen, K. Liu, Y. Xie, M. Lin, and B. Li, *The Partial Discharge Characteristics of Inner Air Gap Inside High-Voltage Cable Termination for High-Speed Trains*, High Voltage, vol. 10, pp. 1110–1124, 2025.

[25] R. Bartnikas, *Partial Discharges: Their Mechanism, Detection and Measurement*, IEEE Transactions on Dielectrics and Electrical Insulation, vol. 9, no. 5, pp. 763–808, 2002.

[26] C. Chen, H. Hsin, C. Hsien, S. Shong, *The Application of On-line PDM on In-service MV Cable Terminations*, IEEE Conference Paper, 2008.

[27] R. Cselkó, Z. Á. Tamus, A. Szabó, I. Berta, *Comparison of Acoustic and Electrical Partial Discharge Measurements on Cable Terminations*, IEEE Conference Paper, 2010.

[28] H. I. Uckol, S. Ilhan, and A. Ozdemir, *Workmanship defect classification in medium voltage cable terminations with convolutional neural network*, Electric Power Systems Research, vol. 194, 2021.

[29] U. Musa, A. A. Mati, A. A. Mas'ud, G. S. Shehu, R. Albarracin-Sanchez, and J. M. Rodriguez-Serna, *Modeling and Analysis of Electric Field Variation across Insulation System of a MV Power Cable*, Proc. of the 3rd International Conference on Electrical, Communication and Computer Engineering (ICECCE), Kuala Lumpur, Malaysia, 2021.

[30] B. N. Gugulothu, S. Lakshminarayanan, M. Palati, S. H. Lakshmegowda, and M. Bukya, *A Study of XLPE Insulation Failure in Power Cables under Electromagnetic Stress*, Engineering Research Express, vol. 6, 2024.

[31] S. S. Desouky, A. Z. El-Dein, R. A. Abd El-Aal, and N. A. A. El-Rahman, *A New Contribution in Reducing Electric Field Distribution Within/Around Medium Voltage Underground Cable Terminations*, Engineering, Technology & Applied Science Research, vol. 7, no. 5, pp. 1962–1966, 2017.

[32] M. Batalović, M. Matoruga, H. Zildžo, and F. Pašalić, *Simulation of Electrical Stress Control System inside Medium Voltage Cable Termination using COMSOL Mph Software Platform*, International Conference on Advanced Technologies (ICAT), 2023.

[33] K. Väkeväinen, *The Effect of Material Properties on Electric Field Distribution in Medium Voltage Underground Cable Accessories*, Degree Thesis, Arcada University of Applied Sciences, 2010.

[34] IEC, *IEC 60502-2: Power cables with extruded insulation and their accessories for rated voltages from 1 kV to 30 kV*, International Electrotechnical Commission, 2014.

[35] NKT, *Universal Cable Catalogue*, 2010.

[36] A. Aarnio, *Electrical Properties of Materials Used in Medium Voltage Cable Accessories*, Master's Thesis, Tampere University of Technology, Finland, 2010.

DEPARTMENT OF ELECTRICAL ENGINEERING
CHALMERS UNIVERSITY OF TECHNOLOGY
Gothenburg, Sweden
www.chalmers.se

CHALMERS
UNIVERSITY OF TECHNOLOGY